Precessional extraction of the K130 cyclotron

Master's Thesis, 3.4.2024

Author:

Timo Ahola

Supervisor:

Taneli Kalvas

UNIVERSITY OF JYVÄSKYLÄ
DEPARTMENT OF PHYSICS

Abstract

Ahola, Timo
Precessional extraction of the K130 cyclotron
Master's thesis
Department of Physics, University of Jyväskylä, 2024, 66 pages.

A simulation study on the extraction from the K130 cyclotron was conducted to see if real life operation of the cyclotron could produce optimal extraction of the particle beam. A python simulation of a simplified K130 was built and two cases were selected to be simulated; $^{15}N^{4+}$ with a target energy of 130 MeV and $^{36}Ar^{7+}$ with a target energy of 140 MeV. For these two cases a particle was simulated for the range of the harmonic coil settings and from these settings some were selected for further analysis based on the final energy and path of the particle. The analysis included simulating the trajectories of beams with finite emittance to find the number of particles, which passed through the deflector, and their energies. From the analysis it was found that the range of the harmonic coil settings that provided optimal output was broad enough to be tunable to by the cyclotron operator, in real life conditions.

Keywords: Cyclotron, extraction, simulation, ion beam, K130

Tiivistelmä

Ahola, Timo
K130 syklotronin prekessionaalinen ekstraktio
Pro gradu -tutkielma
Fysiikan laitos, Jyväskylän yliopisto, 2024, 66 sivua

Tämän tutkimuksen tavoitteena oli selvittää onko K130 syklotronin ekstraktio mahdollista säätää siten, että ekstraktio olisi optimaalinen. Tätä varten rakennettiin python-simulaatio yksinkertaistetusta K130 syklotronista. Simulaatioon valittiin kaksi eri hiukkasta, eri kohde-energioilla; $^{15}N^{4+}$ 130 MeV:n kohde-energialla ja $^{36}Ar^{7+}$ 140 MeV:n kohde-energialla. Näillä kahdelle tapaukselle simuloitiin yksittäisiä hiukkasia, käyden harmonisten kelojen säätöalueen läpi. Näistä simuloiduista tapauksista muutamia valittiin tarkempaan analyysiin, hiukkasten radan ja lopullisen energian perusteella. Analyysissä simuloitiin poikkileikkaus hiukkassuihkusta valituilla harmonisten kelojen säädöillä, jotta säädöt joilla eniten oikella energialla olevia hiukkasia päätyy deflektorista läpi saatiin selvitettyä. Analyysin tuloksena saatiin selville, että syklotronin säätötarkkuus harmonisten kelojen osalta riittää siihen, että operaattori voi säätää suihkun ulostulon optimaaliseksi.

Avainsanat: Syklotroni, ekstraktio, simulaatio, ionisuihku, K130

Contents

1 Introduction

The first cyclotron was created in 1931 by Ernest Lawrence [1]. The design was very simple by today's standards, it had a magnetic field that bent particle trajectories into a circular orbit around the center and electrodes with which the ions were accelerated each turn. Extraction of the ions was made possible by an electrostatic deflector, between two slits, that captured only high energy ions. Even though it has been almost 100 years from the invention of the cyclotron, many of the basic principles still hold true in modern day cyclotrons.

The focus of this study, the extraction in the K130 cyclotron, is also achieved using an electrostatic deflector, like in the first cyclotron by Lawrence. In Lawrence's first cyclotron the particles never exited the cyclotron and the deflector only guided them to a collector inside the cyclotron where they were analysed. Of course the process of extraction is a lot more complex in the K130 as there is a need to get the particles from the cyclotron to the beamline and to the laboratories of the research groups. Unlike in Lawrence's cyclotron, in K130 the magnetic field is not constant and there are harmonic coils further increasing the separation of the final few orbits of the ions. The physical position and the voltage of the deflector can also be adjusted. The complexity of the modern extraction system creates multiple degrees of freedom that complicate the system to the point that the trajectories of the ions cannot be solved analytically, unlike in the early days of cyclotrons. The K130 was designed in the 80s and 90s, when simulating particle trajectories was extremely slow. As such, a study of the extraction could not be done to the level of precision it can be done today. The latest documented update to the extraction was the addition of a negative ion stripper for H^- and D^- ions in 2001 [2]. Before that, the latest update to the positive ion extraction was an update to the deflector materials in 1996 [3]. This obviously poses a question about the optimality of the extraction. Can anything be done to improve the efficiency of the ion extraction process? There could be a lot of potential gains to be found in terms of beam current if the extraction is optimised, since most of the time beam tuning is done by the operator inputting previously used values and maybe adjusting them slightly. This has been the modus operandi

in the past and has worked well enough, but there might be room for improvement. In a system as complex as the cyclotron there is a possibility that the operators are tuning the beam to a local maximum or perhaps due to the multiple degrees of freedom might not find improvement, where there should be. And thus are not utilising the full potential of the cyclotron. With today's computing power finding the actual optimal values for extraction is only a matter of time.

2 Theoretical background

2.1 Basics of cyclotrons

The basis of cyclotrons, or any type particle accelerators, lies in the Lorentz force. Lorentz force makes accelerating and guiding charged particles possible and is therefore crucial for understanding the mechanics of a cyclotron. Starting from basics, we know that the Lorentz force takes the form

$$\mathbf{F} = q\left(\mathbf{E} + \mathbf{v} \times \mathbf{B}\right), \tag{1}$$

where q is the charge of the particle, $\mathbf{E}$ is the electric field, $\mathbf{v}$ is the velocity of the charged particle and $\mathbf{B}$ is the magnetic flux.

This means that charged particles experience a combined force that is comprised of a force acting parallel to the electric field and a force acting perpendicular to the velocity and the magnetic field, which in turn means that one can add energy to the particles using electric fields, but only change direction of the particles using magnetic fields. Also the fact that the force acting on the charged particles due to the magnetic field is proportional to the velocity of the particles, makes it stronger than the force from the electric field. In cyclotrons a big magnet holds the particles in a circular orbit, while the electric fields provide small kicks each orbit that increase the energy of the particle. To achieve similar results with a linear accelerator, one would need either a very high voltage or a very long accelerator with multiple acceleration gaps.

The accelerating force depends only on the charge of the accelerated ions and the strength of the electric field. With modern ion sources, very high charge states can be achieved, thereby increasing the magnitude of acceleration. This combined with simple high-voltage electrodes means that very high energies can be achieved.

From eq. (1) we can derive a few important results. First of all we can find the

turning radius of a particle in a magnetic field with $\mathbf{E} = 0$,

$$\frac{m\mathbf{v}^2}{r} = q(\mathbf{v} \times \mathbf{B}), \tag{2}$$

where m is the mass of the particle and r is the radius of the curvature. Now, assuming that $\mathbf{v}$ and $\mathbf{B}$ are perpendicular we get that,

$$\frac{mv^2}{r} = qvB, \tag{3}$$

$$r = \frac{mv}{qB}. \tag{4}$$

This result also applies relativistically as $m = \gamma m_0$, where γ is the Lorentz-factor and m_0 is the rest mass of the particle. Another important result we can derive from eq. (1) is the cyclotron frequency. The cyclotron frequency is the frequency at which the particles orbit the magnetic field. Starting off similarly to calculating the radius,

$$\frac{mv}{r} = qB, \tag{5}$$

and stating the velocity using angular velocity we get that

$$\frac{m(2\pi f_c r)}{r} = qB, \tag{6}$$

$$m(2\pi f_c) = qB, \tag{7}$$

$$f_c = \frac{qB}{2\pi m}, \tag{8}$$

which importantly is independent of the radius. Applying this frequency, or a multiple of this frequency $f_{acc} = hf_c, h \in \mathbb{N}$, to the accelerating electrodes means that the particles are accelerated every time they are between electrodes. As with the radius, converting this to a relativistic equation requires $m = \gamma m_0$. This causes a problem, since γ is dependent on the particle velocity and therefore the radius and as such, the frequency is also dependent on the radius. If the acceleration frequency is constant and the cyclotron frequency is not, the particles experience sub-optimal, or even negative acceleration, limiting the usefulness of the cyclotron at relativistic energies. There are ways to compensate for this, more on them later.

The absolute maximum energy of a cyclotron arises from the bending limit of the cyclotron. This is the energy at which the magnetic field is unable to hold the

particles in the cyclotron. As the kinetic energy of the particles increases, the radius also increases. The bending limit of a cyclotron gives the energy limit for charged particles due to magnetic bending. To calculate the bending limit, we will start with the turning radius and modify the equation slightly:

$$qBr = p, \tag{9}$$

where $p = \gamma m_0 v$ is the relativistic momentum of the particle and q is the charge of the particle. Now when this is applied to the kinetic energy formula, we get

$$E_k = \frac{p^2}{2\gamma m_0}, \tag{10}$$

$$E_k = \frac{q^2}{2\gamma m_0}(Br)^2, \tag{11}$$

where E_k is the kinetic energy of the charged particle. Using the maximum values for B and the radius at which the maximum B is achieved, we have a result that is unique to each cyclotron. Using these values and grouping all the constants we get

$$\frac{E_k}{M} = K\frac{Q^2}{M^2}, \tag{12}$$

where Q is the charge number of the ion, K is all the constants and $M = m_0/m_u$ the mass of the atom in atom mass units. For protons this equation is essentially $E_k = K$. Since K is unique to each cyclotron, they are often named after this energy e.g. K130 cyclotron for which $K = 130$ MeV in Jyväskylä and K1200 at MSU for which $K = 1200$ MeV. The K-energy directly indicates the maximum limit energy the cyclotron can achieve for a given particle. However, in practice there are more limitations to consider, which might make it not possible to reach the absolute maximum energy.

In the real world the trajectories of the particles are never perfect and are subject to small changes in initial conditions. This causes the orbit of the particle to not return to the same position after each turn even if there is no acceleration. Due to the focusing properties of cyclotrons, these small changes in initial conditions lead to oscillation around the ideal orbit, also called the equilibrium orbit [4]. These oscillations have specific frequencies called betatron frequencies and they can be in

the radial or axial directions. These oscillations occur at frequencies

$$f_r = \sqrt{1-k} f_c, \tag{13}$$

$$f_z = \sqrt{k} f_c, \tag{14}$$

where k is the field index

$$k = \frac{r}{B}\frac{dB}{dr}, \tag{15}$$

and f_r and f_z are radial and axial oscillation frequencies respectively. [4] These oscillations are usually expressed relative to the cyclotron frequency

$$\nu_r = \frac{f_r}{f_c}\sqrt{1+k}, \tag{16}$$

$$\nu_z = \frac{f_z}{f_c}\sqrt{-k}. \tag{17}$$

The cyclotron is focusing in both planes if the value of k is $-1 < k < 0$ [4]. This means that the field must be radially decreasing for focusing to occur.

As the particles are accelerated in a cyclotron, they oscillate around the equilibrium orbits. This oscillation of the particles affects the separation of each turn. The radial position for the particle at any azimuth θ can thus be calculated by taking into account the radial position change due to the increase in energy, shape of the equilibrium orbit and the oscillation around the equilibrium orbit. The radial position can be expressed as [5]

$$r(\theta) = r_0(\theta) + x(\theta)\sin(\nu_r\theta + \theta_0), \tag{18}$$

where $r_0(\theta)$ is the equilibrium orbit radius at angle θ, $x(\theta)$ is the amplitude of the sinusoidal oscillation around the equilibrium orbit and θ_0 is the phase angle of the oscillation. From this, one can calculate the radius at turn number n as

$$r(\theta_n) = r_0(\theta_n) + x(\theta)\sin(2\pi n(\nu_r - 1) + \theta_0), \tag{19}$$

where θ_n is a constant angle at the start of each turn. Since ν_r is close to one it is convenient to use $\nu_r - 1$. [5] By differentiation one can derive the turn separation for

two successive turns to be

$$\begin{aligned}\Delta r(\theta_n) =&\Delta r_0(\theta_n) + \Delta x(\theta_n)\sin\left(2\pi n(\nu_r - 1) + \theta_0\right) \\ &+ 2\pi(\nu_r - 1)x(\theta_n)\cos\left(2\pi n(\nu_r - 1) + \theta_0\right).\end{aligned} \tag{20}$$

The first term is the separation due to increase in energy. The second term gives the amount of separation due to the change in oscillation amplitude around the equilibrium orbit Δx. The oscillation amplitude can be controlled with magnetic field disturbances. These disturbances can be created using well placed coils in the cyclotron, called harmonic coils. The third term gives the turn separation due to the oscillation around the equilibrium orbit. Do note that if $\nu_r = 1$, only the change in energy has an effect on the radius, however any acceleration that takes the particles out of an equilibrium orbit affects ν_r, so $\nu_r = 0$ only in ideal circumstances. [5] Figure 1 was made to show the effects on the radius of a particle separately.

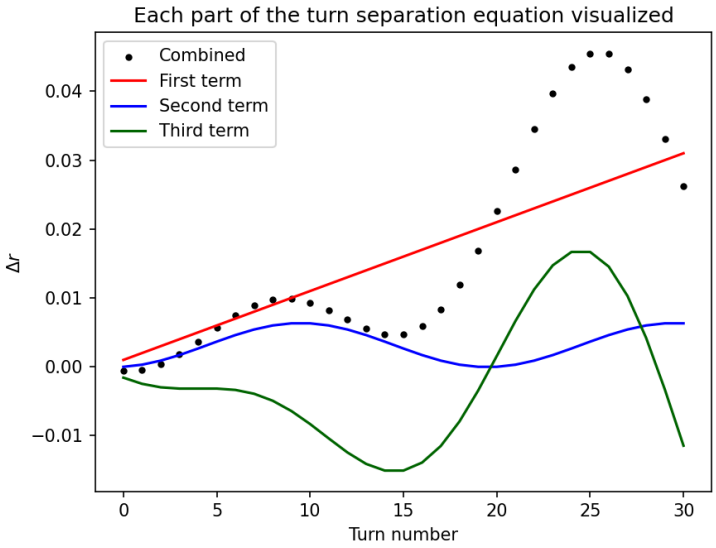

Figure 1. A figure showing the contribution to the change in radius for each part of eq. (20). The angle at each turn is constant and the radial units in the figure are arbitrary. The change in oscillation amplitude Δx, is constant. In the figure one can see the effect of the amplitude change on the sinusoidal oscillation around the equilibrium orbit. The change in radius due to acceleration is small compared to the fluctuations caused by the oscillation.

2.2 Isochronous cyclotron

Cyclotrons fall into three general categories: Classical cyclotrons that operate very much alike the first cyclotrons, synchrocyclotrons that account for relativistic effects by altering the acceleration frequency, and finally isochronous cyclotrons that, instead of altering the acceleration frequency, have a radially increasing magnetic field, which keeps the cyclotron frequency constant.

Classical cyclotrons are the most simple type of cyclotron and are best at low energy applications. Synchrocyclotrons can accelerate the particles to the highest energies, but can only accelerate a few bunches at a time so they can only produce relatively low intesity beams. Isochronous cyclotrons are most fitting for high power applications since they can accelerate a quasi-continuous beam to high energies, but they are more complex than other types due to the requirements of the magnetic field.

An isochronous cyclotron has an azimuthally and radially varying magnetic field. The magnetic field increases with radius to make the particles orbit the center of the cyclotron at a constant frequency. The azimuthal variation induces focusing of the beam by having high- and low -field sectors, called “hills” and “valleys”. The sector borders produce a focus-defocus-focus chain for an overall focusing effect. [6]

For the isochronous cyclotron to work, the cyclotron frequency, eq. (8) must be constant for all radii, so that

$$f_c = \frac{qB(r_1)}{2\pi\gamma_1 m_0} = \frac{qB(r_2)}{2\pi\gamma_2 m_0}, \tag{21}$$

where r_1 and r_2 are any two radii inside the cyclotron and γ_1 and γ_2 are the Lorentz-factors at corresponding velocities. When this is true, the acceleration can be done with a constant RF frequency and multiple pulses can be accelerated at the same time. In reality at some points the frequency is not exactly the same, which induces a phase error. This can be corrected by having a phase error in the other direction later. In cyclotrons that operate at multiple energies and can accelerate many different particles, the phase error correction is usually done by tuning the magnetic field with multiple coils with different radii, called trim coils, so that the integrated phase error is minimised. An example of the phase error can be seen in figure 2.

Assuming that $r_1 < r_2$ and, as energy increases radially, $\gamma_1 < \gamma_2$, we can find out

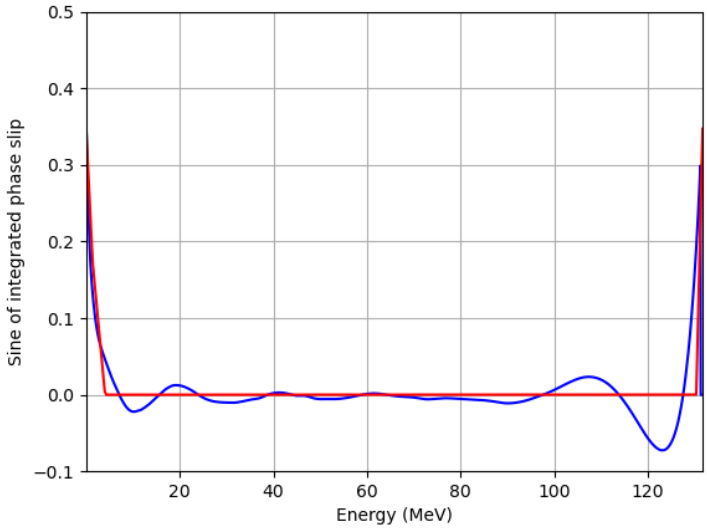

Figure 2. Red line describes the ideal phase and the blue line is the actual phase. The integrated phase error mostly stays near the ideal error, but at some points going over or under. The particle used is $^{15}N^{4+}$ and maximum energy is 130 MeV. The integrated phase error seen here is calculated for the K130 cyclotron.

how $B(r)$ behaves as function of radius. Rearranging eq. (21) we get

$$\frac{\gamma_2}{\gamma_1}B(r_1) = B(r_2). \tag{22}$$

And as previously stated $\gamma_1 < \gamma_2$, leading to $B(r_1) < B(r_2)$, meaning that the field must be increasing radially. This contradicts the fact that focusing in the cyclotron comes from the field decreasing, so there must be another solution. This where the azimuthally varying field with the overall focusing effect of it comes in. From eq. (21) we get that

$$B(r) = \frac{\gamma m_0 2\pi f_c}{q} = \frac{\gamma m_0 \omega_c}{q}, \tag{23}$$

where ω is the angular velocity of the particle. Now using $B_0 = m_0\omega_c/q$,

$$B(r) = \frac{B_0}{\sqrt{1-(\frac{v}{c})^2}} = \frac{B_0}{\sqrt{1-(\frac{r\omega_c}{c})^2}}, \tag{24}$$

where v is the velocity of the particle and B_0 is the magnetic field when not taking

into account relativistic effects. Now substituting this to eq. (15), we get

$$k = \frac{rB_0}{B}\frac{d}{dr}\left(1 - \left(\frac{r\omega_c}{c}\right)^2\right)^{-1/2}, \tag{25}$$

which, when differentiated, gives

$$k = \frac{rB_0}{B}\frac{\omega^2 r}{c^2}\left(1 - \left(\frac{r\omega_c}{c}\right)^2\right)^{-3/2}. \tag{26}$$

Then simplifying this we get

$$k = \frac{1}{\gamma}\frac{\omega^2 r^2}{c^2}\gamma^3 = \frac{1}{\gamma}\beta^2\gamma^3, \tag{27}$$

and finally, using $\beta^2 = 1 - 1/\gamma^2$

$$k = \gamma^2 - 1. \tag{28}$$

Now with the field index for an isochronous cyclotron we can calculate the focusing condition for an isochronous cyclotron. To approximate the betatron frequencies in an isochronous cyclotron flutter is needed. The flutter is a function that expresses the strength of the azimuthal magnetic field variation in a cyclotron. This can then be used to approximate the radial and axial betatron frequencies of the beam ν_r and ν_z. The flutter is defined as

$$F(r) = \frac{\left\langle \mathbf{B}^2 \right\rangle - \langle \mathbf{B} \rangle^2}{\langle \mathbf{B} \rangle^2}, \tag{29}$$

where, $\langle \mathbf{B} \rangle$ is the average of the magnetic field at radius r and $\left\langle \mathbf{B}^2 \right\rangle$ is the average of the squared magnetic field. [7] With flutter the approximations for ν_r^2 and ν_z^2 become

$$\nu_z^2 \approx -k + \frac{N^2}{N^2 - 1}F(1 + 2\tan^2\alpha), \tag{30}$$

$$\nu_r^2 \approx (1 + k) + \frac{3N^2}{(N^2 - 1)(N^2 - 4)}F(1 + \tan^2\alpha), \tag{31}$$

where N is the number of sectors in the cyclotron and α is the spiral angle of the

sectors [7]. Now substituting eq. (28) into these equations we have,

$$1 - \gamma^2 + \frac{N^2}{N^2 - 1} F(1 + 2\tan^2\alpha) > 0, \tag{32}$$

$$\gamma^2 + \frac{3N^2}{(N^2 - 1)(N^2 - 4)} F(1 + \tan^2\alpha) > 0, \tag{33}$$

and finally the conditions become

$$\frac{N^2}{N^2 - 1} F(1 + 2\tan^2\alpha) > \gamma^2 - 1, \tag{34}$$

$$\frac{3N^2}{(N^2 - 1)(N^2 - 4)} F(1 + \tan^2\alpha) > -\gamma^2, \tag{35}$$

for z and r -plane focusing respectively.

2.3 Extraction

Extraction from a cyclotron is not as simple as one might think. At some radius in an isochronous cyclotron the average magnetic field starts to decrease and this induces more phase error for the particles while still keeping them on a circular orbit. This will affect the particle trajectories and make them more difficult to extract. For this reason it is imperative that the particles are extracted before they get to such a radius. To accomplish this one needs to have some way to quickly increase the radius of the particles to outside the cyclotron. In a system that is prone to chaos, this requires some sort of precise disruption of the trajectories.

The simplest way of extracting particles is using a stripper foil, usually carbon, to strip electrons off of negative ions, thus changing their charge and reversing the direction of the force bending the ions. This is used widely in commercially available cyclotrons due to the simplicity, compactness and high efficiency. The high efficiency also means there is less activation of the cyclotron components, making it safer to work on. [8, 9]. This method is used for accelerating H^- and D^- ions.

Another way is to use coils to create harmonic disturbances in the magnetic field of the cyclotron. This alters the turn separation by changing the amplitude of the precession as demonstrated in eq. (20). Using harmonic coils and an electrostatic deflector increases the degrees of freedom in the system and therefore makes tuning for maximal efficiency possible. The downside is that the system becomes more complex and requires precise tuning. In a cyclotron harmonic coils can be used to

increase turn separation and therefore make extraction easier. Once the harmonic coils have increased the turn separation the particles will enter the deflector which increases the radius of the particles and guides them into the electromagnetic channel which further increases the radius of the particles by opposing the magnetic field of the cyclotron locally. Once through, the particles are outside the influence of the magnetic field of the cyclotron and are guided along the beamline. This method is not as efficient, compact or simple as the stripping extraction, but it will work for basically any positively charged particle. An example of the final few turns with this extraction type can be seen in figure 3.

There is also a relatively new method of extraction by acceleration, where an isochronous cyclotron was designed to be operated without a deflector [10]. The extraction is based on having a very narrow gap between the magnets and increasing the gap suddenly at the point of extraction. This causes an abrupt decrease in the magnetic field to the point where the magnetic field cannot hold the particles in the cyclotron. This abrupt decrease makes the extraction controllable unlike the slow decrease usually found in isochronous cyclotrons. [11]

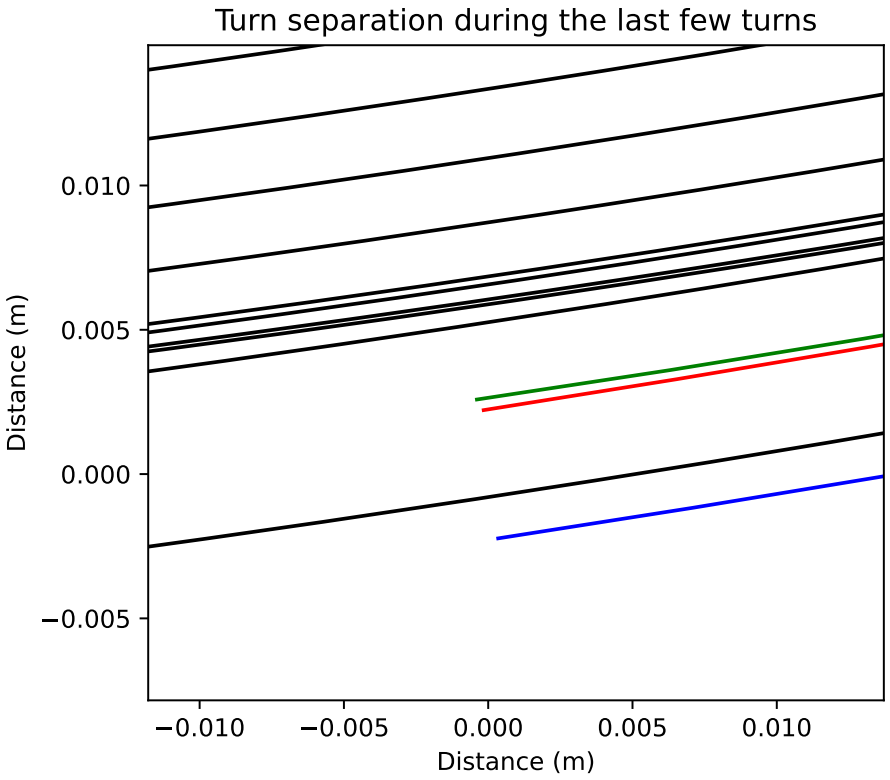

Figure 3. The turn separation during the last few turns. Black line is the particle trajectory and colored lines give the outlines of the deflector. The turn radius increase is roughly constant before these turns. Note that on the final turn the turn separation is very large. Comparing to figure 1, the orbit radii seem to behave quite similarly in some areas, with orbits bunching up before having a large turn separation for the last one. However no definite conclusion should be drawn from this, as figure 3 shows a much simpler version of the radial separation.

3 Methods and materials

3.1 The K130 cyclotron

The K130 cyclotron at the University of Jyväskylä has been in constant use since 1994. The cyclotron is an AVF-cyclotron (Azimuthally varying field). The structure used to produce the magnetic field consists of the main electromagnet, three 58° spiral sectors, 15 pairs of trim coils, used to tune the magnetic field, and 4 sets of three harmonic coil pairs at different radii. The acceleration is done with two dee electrodes and two ground electrodes. On each turn the particles are accelerated in 4 acceleration gaps. [12] The K130 is used with harmonic numbers 1,2, and 3, with an RF-frequency of 10–21 MHz. The maximum field at the extraction radius, averaged over all azimuth angles the main electromagnet can produce, is 1.76 T [13]. The acceleration voltage is 50 kV at maximum. Most of the trim coils can have currents between −100 A and 100 A, with a few coils having more limited ranges. The harmonic coils have currents between −5 A and 5 A. The harmonic coils are tuned by assigning a single value of current and an angle, with the precision of the current being 10 mA and angle adjustment being 1°. The currents for the coils are then calculated as

$$I_1 = I_{set}\cos(\theta) \tag{36}$$

$$I_2 = I_{set}\cos(\theta + 120^\circ) \tag{37}$$

$$I_3 = I_{set}\cos(\theta - 120^\circ) \tag{38}$$

with θ being the angle set, and I_x being the current of the coil and I_{set} being the current the operator sets. The voltage of the electrostatic deflector can be set between 0 and 60 kV and also the position and angle of the deflector can be adjusted at the entrance and the exit. Both of these can be adjusted by 4 cm radially with 0.5 mm precision. The width of the entrance is roughly 4.5 mm and the width of the exit is roughly 6.3 mm

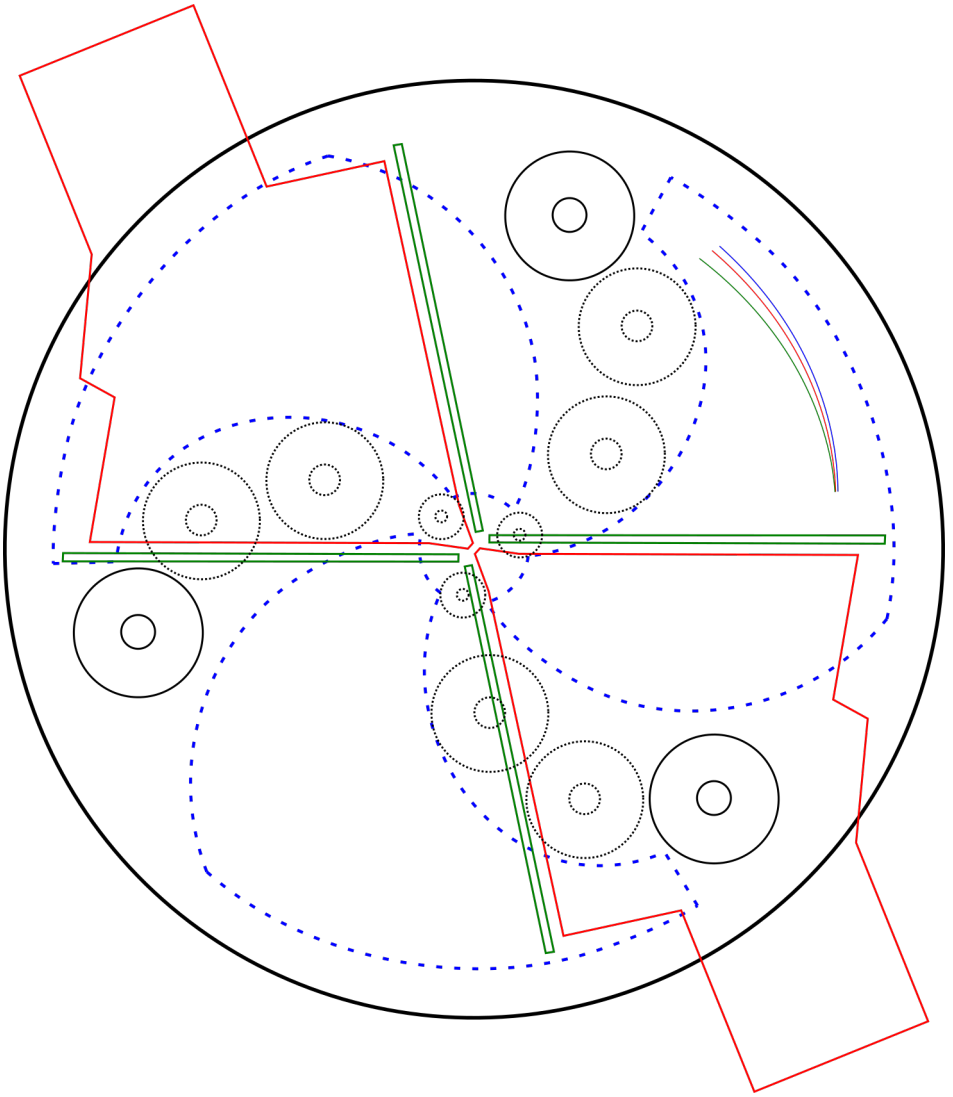

Figure 4. A schematic of the K130 cyclotron. Red blocks are the dee-electrodes, green are the edges of the dummy dees, dashed blue lines show the magnetic sectors, black circles are the harmonic coils of which the outermost are important in extraction. And the multiple colored lines in the top right hand corner of the cyclotron give the outlines of the deflector.

3.2 Magnetic field

The magnetic field was calculated from the output of the field trimming program Fielder [14]. The input consists of particle mass, charge and the energy or main coil current. From these Fielder calculates the main coil current, if necessary, the trim coil currents, the acceleration frequency and voltage, as well as the harmonic number. Also the magnetic field and trim coil fields are output. With these one can calculate a full field of the cyclotron. For the harmonic coils, Opera simulation software [15] was used to calculate the harmonic coil fields. The harmonic coil fields were simulated with multiple main coil current values. This was done to account for the change in permeability of the coils caused by the main magnetic field. The simulations were done with one harmonic coil at 5 A and 0 A. The resulting magnetic field was then assumed to behave linearly, so that the full range of current from -5 A to 5 A could be interpolated. Since all three outermost coils are identical and in essentially identical sectors, this one result was then copied and shifted 120° and $-120°$ to make up three identical harmonic coil pairs, with each pair having their own current. The coil fields were tested to verify that the shifting of the fields does not induce errors that affect the end result of the simulation. There might be a difference between the numbering of the harmonic coils in the simulation and the real cyclotron as it is not known which of the three coils is number one in the real cyclotron. This only means that the harmonic coil angles from the simulation might be offset by 0, ± 120 or ± 240 degrees, compared to real life.

As the coordinates of the cyclotron are different in Fielder and Opera a rotation of -88° was done for the field from Fielder. In the original schematics the angle of the deflector entrance is 10° and in the coordinates of Opera, the deflector is at 8°. Fielder has the deflector at 280°, therefore a rotation of the field by 270° or $-90°$ gives the field in the original schematics coordinates and a rotation of 272° or $-88°$ gives the same coordinates as Opera. These coordinates are then used for everything in the simulation. Figures 8a, 8b, 8c and 8d show the differences between the fields from Opera and Fielder and how well a rotated field from Fielder matches the field from Opera.

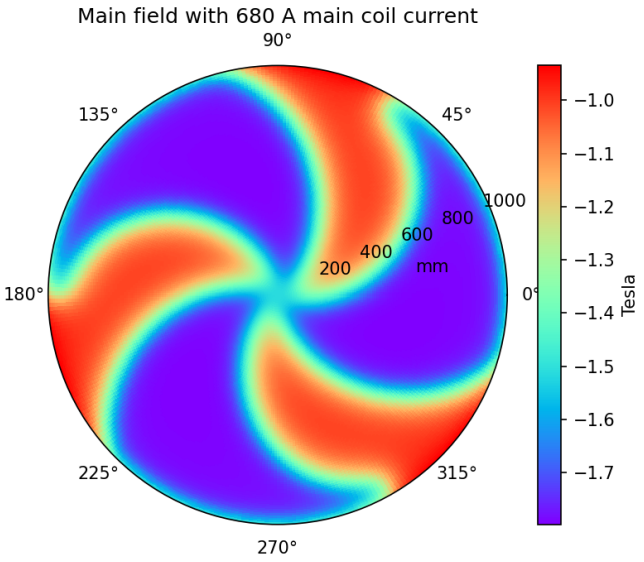

Figure 5. The magnetic field caused by the main coil. Here one can clearly see the spiral structure of the sectors affecting the magnetic field.

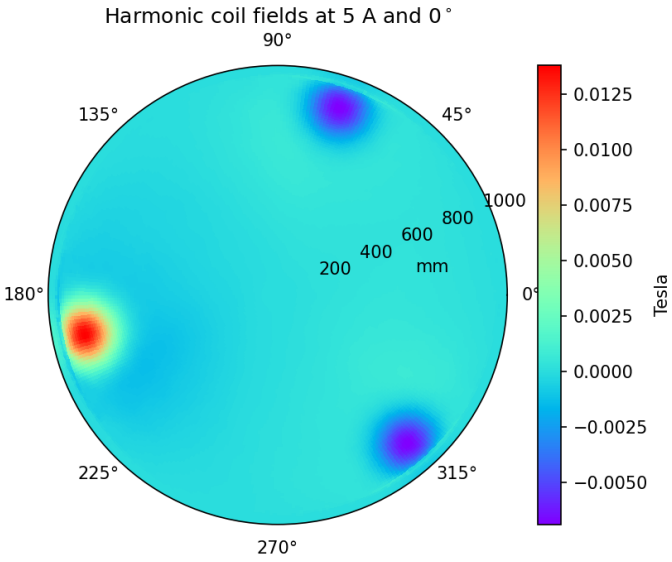

Figure 6. The magnetic fields of the outermost harmonic coils. When the coils have a positive current they oppose the main magnetic field. The fields of the harmonic coils even at maximum current are only a fraction of the main coil field.

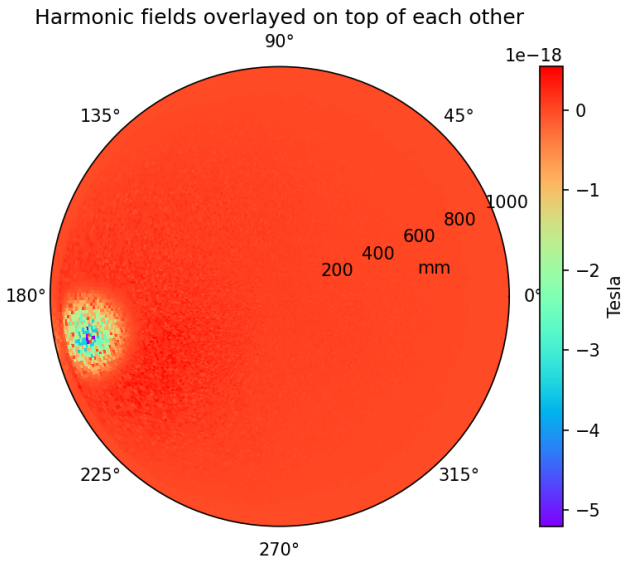

Figure 7. The fields from each coil overlayed on top of one another. As the currents of the coils sum up to zero this should produce a 0 T magnetic field. As one can see the resulting field is not exactly zero but is small enough compared to the other fields that it is practically so.

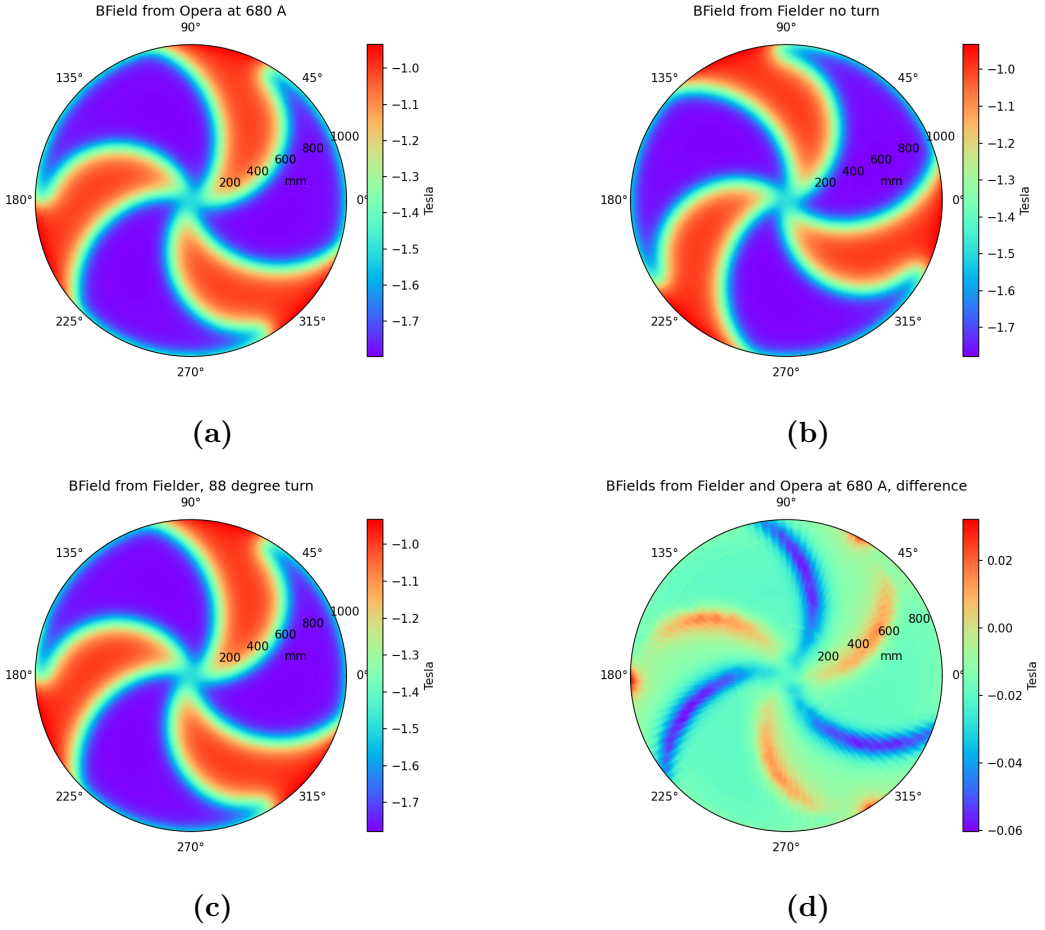

Figure 8. Figures showing the magnetic field from Opera, the magnetic field output by Fielder, the rotated field from Fielder and the difference between the field from Opera and the rotated field from Fielder. The rotation of the field from Fielder is not quite perfect and interpolation might play a part in giving the ideal turn angle. In this case the ideal turn angle would be around 87.5°. In the end the field in the simulation was rotated 88°, since that rotation did not require interpolation and matched the field from Opera quite well.

3.3 Equations of motion

The particle trajectories are calculated in cartesian coordinates in two dimensions, corresponding to the transverse plane of the cyclotron. The axial direction was ignored since it has little effect in the precessional extraction. This is due to the magnetic field essentially being in the axial direction and therefore the forces caused by it are in the transverse plane. Also the introduction of a third dimension would slow down the simulation. Since the energies of the particles in an isochronous cyclotron are in the relativistic regime the equations of motion have to take relativistic effects into account. The equations of motion form a matrix equation, that is then solved using `numpy.linalg.solve` [16] method.

Starting off with the Lorentz force from eq. (1), and assuming that the velocity is relativistic, we first have

$$\frac{d\mathbf{p}}{dt} = q(\mathbf{E} + \mathbf{v} \times \mathbf{B}), \tag{39}$$

where the force is expressed as the time differential of momentum, which can be stated as

$$\frac{d\mathbf{p}}{dt} = \frac{d}{dt}(\gamma m \mathbf{v}), \tag{40}$$

where m is the particle mass. Now taking the right sides of the equations we have

$$\mathbf{v}\frac{d\gamma}{dt} + \gamma\frac{d\mathbf{v}}{dt} = \frac{q}{m}(\mathbf{E} + \mathbf{v} \times \mathbf{B}), \tag{41}$$

where

$$\gamma = \frac{1}{\sqrt{1 - \frac{|\mathbf{v}|^2}{c^2}}}. \tag{42}$$

Now calculating the derivative of γ we get

$$\frac{d\gamma}{dt} = -\frac{1}{2}\frac{1}{\left(1 - \frac{|\mathbf{v}|^2}{c^2}\right)^{3/2}}\frac{2|\mathbf{v}|}{c^2}\frac{d|\mathbf{v}|}{dt} \tag{43}$$

Which can be written as

$$\frac{d\gamma}{dt} = \gamma^3\frac{|\mathbf{v}|}{c^2}\frac{d|\mathbf{v}|}{dt}. \tag{44}$$

Now differentiating $d|\mathbf{v}|/dt$ component by component we have

$$\frac{d|\mathbf{v}|}{dt} = \frac{1}{2}\left(v_x^2 + v_y^2 + v_z^2\right)^{-\frac{1}{2}}\left(2v_x\frac{dv_x}{dt} + 2v_y\frac{dv_y}{dt} + 2v_z\frac{dv_z}{dt}\right) \tag{45}$$

which comes to be

$$\frac{d|\mathbf{v}|}{dt} = \frac{v_x\frac{dv_x}{dt} + v_y\frac{dv_y}{dt} + v_z\frac{dv_z}{dt}}{\sqrt{v_x^2 + v_y^2 + v_z^2}} = \frac{v_x\frac{dv_x}{dt} + v_y\frac{dv_y}{dt} + v_z\frac{dv_z}{dt}}{|\mathbf{v}|}. \tag{46}$$

Now substituting this into eq. (44) we get that

$$\frac{d\gamma}{dt} = \gamma^3\frac{v_x\frac{dv_x}{dt} + v_y\frac{dv_y}{dt} + v_z\frac{dv_z}{dt}}{c^2}. \tag{47}$$

And now again substituting into eq. (41) we get

$$\mathbf{v}\gamma^3\frac{v_x\frac{dv_x}{dt} + v_y\frac{dv_y}{dt} + v_z\frac{dv_z}{dt}}{c^2} + \gamma\left(\frac{dv_x}{dt}\hat{x} + \frac{dv_y}{dt}\hat{y} + \frac{dv_z}{dt}\hat{z}\right) = \frac{q}{m}(\mathbf{E} + \mathbf{v}\times\mathbf{B}). \tag{48}$$

Now we can form a matrix differential equation, which is in form

$$\begin{bmatrix} v_x\gamma^3\frac{v_x}{c^2} + \gamma & v_x\gamma^3\frac{v_y}{c^2} & v_x\gamma^3\frac{v_z}{c^2} \\ v_y\gamma^3\frac{v_x}{c^2} & v_y\gamma^3\frac{v_y}{c^2} + \gamma & v_y\gamma^3\frac{v_z}{c^2} \\ v_z\gamma^3\frac{v_x}{c^2} & v_z\gamma^3\frac{v_y}{c^2} & v_z\gamma^3\frac{v_z}{c^2} + \gamma \end{bmatrix}\begin{bmatrix} \frac{dv_x}{dt} \\ \frac{dv_y}{dt} \\ \frac{dv_z}{dt} \end{bmatrix} = \frac{q}{m}\begin{bmatrix} E_x + v_yB_z - v_zB_y \\ E_y + v_zB_x - v_xB_z \\ E_z + v_xB_y - v_yB_x \end{bmatrix}. \tag{49}$$

The matrix form equation of motion is then calculated using `numpy.linalg.solve`. The solution returns dv/dt for each vector component. Note that in the simulation B_x, B_y and E_z are set at zero and thus the problem reduces to

$$\begin{bmatrix} v_x\gamma^3\frac{v_x}{c^2} + \gamma & v_x\gamma^3\frac{v_y}{c^2} \\ v_y\gamma^3\frac{v_x}{c^2} & v_y\gamma^3\frac{v_y}{c^2} + \gamma \end{bmatrix}\begin{bmatrix} \frac{dv_x}{dt} \\ \frac{dv_y}{dt} \end{bmatrix} = \frac{q}{m}\begin{bmatrix} E_x + v_yB_z \\ E_y - v_xB_z \end{bmatrix}. \tag{50}$$

3.4 Integration

Integration is done using `RK45` method from `scipy.integrate` [17] library. The start of the integration was set arbitrarily at 270° so that crossing the y-axis from negative x to positive x was a complete orbit. The integration routine takes in the time derivatives for the position and velocity for each coordinate and integrates them, giving position and velocity of the particle at the next time step. The time step is variable, but for the deflector the time step is constrained artificially for better accuracy. In the deflector the maximum time step is 10^{-11} s which translates to a positional step of around 0.3 mm at 55 MeV with $^{15}N^{4+}$ and 0.4 mm at 130 MeV with the same particle. In the acceleration gaps the time step is not constrained. This has a small effect on the energy of the particles but not a major one. In 10 orbits with maximum time step of 10^{-10} s vs 10^{-11} s, the difference in gained energy is between 1 keV and 10 keV with the energy gain being around 5 MeV and starting energy of 55 MeV with acceleration voltage of 31.9 kV and acceleration frequency of 13.8782 MHz with harmonic number 2. This gives an error of around 0.1%. Meanwhile the time it takes to calculate the trajectories for 10 orbits increases from around 10 s to 100 s, a tenfold increase. This error in energy is acceptable considering the time it saves to integrate with a larger time step. For reference integrating $^{15}N^{4+}$ from 55 MeV to 130 MeV takes around 150 orbits. Considering a tenfold increase in integration time, the time saved per full trajectory integration would be roughly 1350 s or 22.5 minutes (150 s vs 1500 s). These calculations were made with an AMD Ryzen™ 7 2700 CPU.

3.5 Initial conditions

The initial conditions, from which the calculation of the particle trajectories is started, was selected to be in a section of the cyclotron where there are no electric fields or harmonic coil interference. These could have an undesired effect on the rest of the calculation and could induce errors. Therefore the starting place was selected to be roughly half the radius of the cyclotron, away from the acceleration gaps. Close to the center where the inflector is located, electric fields are used to control the beam. Starting from half the radius also simplifies the acceleration gaps since the dees of the cyclotron are not perpendicular to the dummy-dees near the center.

Using data obtained from Fielder, i.e. the energy and radius of the particle, an

initial guess is formed for the initial conditions. From the energy a velocity for the particle is calculated and set so that the direction is in the positive x-direction. The radius is input as negative y-value for the particle to start at 270°. The orbit is then optimized twice, first by minimizing the distance between the end position and starting position after a turn. The result from this is then considered as the initial guess for the second minimization, which minimized the difference in y-velocities at the start of an orbit and at the end. This in effect also minimizes the difference in x-velocities since they are calculated from the energy and therefore are dependent variables. Each minimization ran for 300 orbits for optimal results. Both minimization routines had three values they could change: the starting radius with bounds 0.7 m to 0.3 m, the total velocity of the particle with bounds 95% to 105% of the initial guess velocity and the angle to control the direction of the velocity with bounds 0° to 15°. The bounds were set arbitrarily, but were formulated conservatively so that unintended results would not be possible. The minimization routine most likely does not need to be this complex, but it has verifiably worked for the purposes of this study.

3.6 Deflector

The deflector was modeled using a data sheet from when the cyclotron was built. The data sheet contains three sets of points in two dimensions that describe the curves of the walls of the deflector. These points are then translated into a coordinate system where the center of the entrance to the deflector is at (0, 0). A seventh degree polynomial is then fitted to these points, which then is used as an approximate function to calculate the coordinates of the wall at any position. The first set of points contain the coordinates for the wall that is towards the cyclotron center, the second contain the coordinates for the inner wall of the deflector channel and the third contain the coordinates of the outer wall of the deflector channel. The points can be seen plotted in figure 9.

To calculate the electric field the particles experience between the electrodes, the deflector was assumed to be like a capacitor with the electric field lines pointing from the inner channel wall to the outer at the shortest distance, this being roughly directed along the normal angle of the inner channel wall. The distance between the channel walls is continuously increasing so a calculation of the electric field is required. It is assumed that the electric field does not depend on the distance

between the particle and the channel walls, so that

$$E = \frac{V}{d}, \tag{51}$$

where E is the electric field, V is the voltage between the capacitor walls and d is the distance between the channel walls.

The particle location is first transformed into the same coordinate system as the deflector. Then the shortest distance between the particle and the inner and outer channel walls is found. As the curves of the wall are shallow enough, the shortest distance from inner to outer channel wall is the same, or at least very nearly the same, as the distances from the particle to the walls summed. This makes the calculation easier as there is no need to find a different line. The closest points on the wall are then used to calculate the angle of the electric field.

There are also checks in place to see when the particle has entered the deflector, exited the deflector or collided with a wall in the deflector. In the case that the particle has exited or collided with the walls, the integration is stopped.

The channel in the real deflector is not flat as the distance between the electrodes varies with the z-coordinate. The electrodes are convex in shape. This was chosen to be ignored as this study was meant to examine the harmonic coils and having an ideal deflector makes it much easier. So the decision was made that the distance between the electrodes in the simulation is the same as the distance at the center of the z-axis in the real electrodes of the deflector.

3.7 Acceleration gaps

The acceleration gaps were first simulated in FEMM [18] as a cross section with dimensions from the actual cyclotron as seen in figure 10. The simulation was done using the maximum voltage of 50 kV. Then the electric field as a function of the distance along the particle trajectory was exported from the simulation. A gaussian curve was fitted to the data points from the simulation. As can be seen in figure 11, the fields match quite well when the field is high and is responsible for most of the acceleration. Note that the curve from FEMM is not smooth, with noise arising from the meshing used in the calculation. The gaussian can be scaled linearly to any field corresponding to a voltage between 0 and 50 kV. Since the curve is symmetrical only half of it is used for calculating the electric field the particle experiences. The

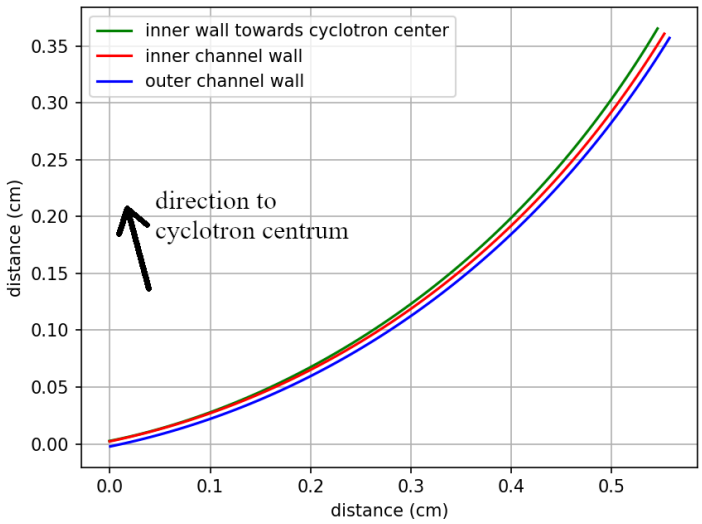

Figure 9. A figure showing the coordinates of the deflector in the simulation. Note that the coordinates are different for the deflector and the general simulation. This is done to make the calculation of the particles in the deflector more simple. The outside of the blue line is considered to be the wall of the cyclotron. The direction of the arrow is approximate. The approximate location inside the cyclotron can be seen in figure 4.

distance between the particle and the center of the accelerating gap determines the strength of the electric field. The gaussian of the electric field was set up so that the particle experiences the highest electric field when it is in the center of the acceleration gap. When the distance of the particle to the center of the acceleration gap is greater than 6 cm, the electric field is automatically set to 0. In actuality the electric field at this point is under 10^4 V/m with FEMM and 10^3 V/m in the gaussian fit with the field in the middle being over 10^6 V/m in both cases. The direction of the acceleration gap field is constant. In reality this is not the case near the center, but since there is no need to simulate particles near the center this approximation is valid.

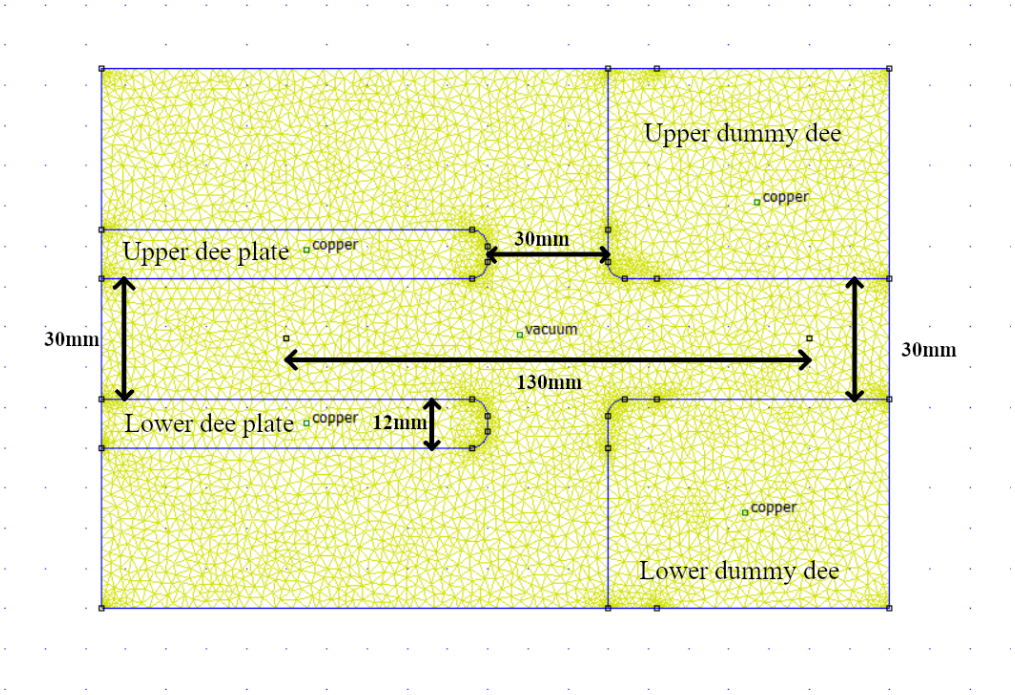

Figure 10. The cross sectional simulation of an acceleration gap. The view is from the side of the cyclotron with the middle plane being where the particles are traveling. The left copper blocks represent the top and bottom of the dee and the right side represents the dummy dee. The electric field is analyzed between the two points between the top and bottom dee and dummy dee, with a distance between the points being 130 mm.

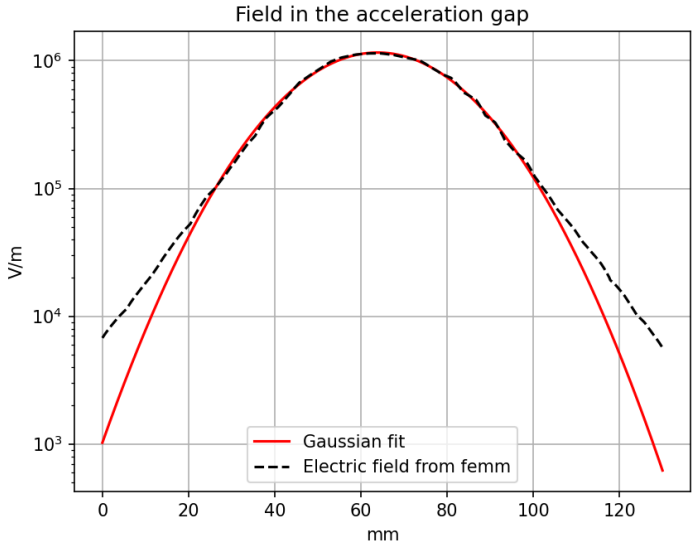

Figure 11. The gaussian electric field used in the simulation and the FEMM simulated version. To get a perfectly smooth electric field a gaussian fit was used. This gets rid of the noise created by the mesh calculation and is simple to implement in the simulation.

3.8 Steps for analysis

First thing to do for the analysis was to find an equilibrium orbit from which to start the integration. The method is described in section 3.5. This was done using a maximum time step of 10^{-11} s to ensure good accuracy. After the initial conditions were found, a sweep through the harmonic coil settings was performed. A maximum time step of 1.5×10^{-10} s was used and the sweep went through the settings 1° and 0.5 A at a time, from $0 - 360°$ and $0 - 5$ A. This produced 3600 unique combinations which were further trimmed to include only those that had a particle go in the deflector. From these combinations a plot was made showcasing the distance to the deflector center as a function of both the angle and current of the harmonic coils. A cutoff was then chosen for the distance and anything under it underwent the next step of analysis. This consisted of first finding an optimal angle for the deflector, so that the particle comes out at the center of the deflector. An example of how this affects the deflector is in figure 12. After this a particle from the initial equilibrium orbit will enter the deflector near the center of the entrance and exit near the center of the exit. This was followed by calculating how many particles in a beam ellipse would go through the deflector with these settings. The beam ellipse consisting of 24

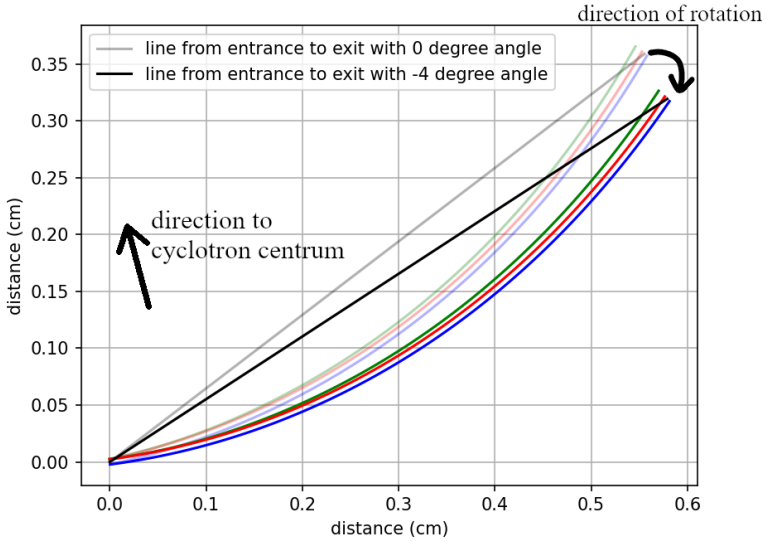

Figure 12. An example figure how the deflector is turned. The entrance position stays the same, since changing it could change particle energies at the end and add unneeded complexity to the analysis. The direction of the arrow is approximate.

particles was formed around the initial equilibrium orbit. The path of these particles was then calculated through the cyclotron. It was checked how many particles went through the deflector and what their energies were. The best solution from these is the one that has the most particles going through the deflector as close to the target energy as possible.

4 Results

4.1 Nitrogen at 130 MeV

The first simulation was done using $^{15}N^{4+}$ with a target energy of 130 MeV. This was done to test that the simulation worked and check if the results it provided seemed realistic. The simulations were done as explained in section 3.8 and the code necessary for analysis was written as needed.

The accuracy of the simulation was compared to output from Fielder, which gave radii at different energies and the average energy gain per turn. The values of the simulation matched Fielder quite well giving a similar number of turns, depending on the settings of the harmonic coils. With this the first step is to do a sweep of the harmonic coil settings, providing us with the energy and distance to the center of the deflector for each particle that goes in the deflector. Note that some particles hit the inner wall of the deflector, therefore making them unable to reach the extraction. The harmonic coil sweeps are seen in figures 15 and 16. The particle data can be found in appendix A table 1. A thing of note is that the range of the energies of the particles is quite big at around 6 MeV, which corresponds to 12 orbits in this case.

This data was then filtered to include only the lowest values for distance to the entrance of the deflector. The cutoff was a distance of 0.374 mm from the entrance to the deflector, which included 30 cases. For each of these cases an optimal angle of the deflector was calculated with the voltage in the deflector being 20 kV. The cutoff distance was chosen arbitrarily to limit the number of cases. It was assumed that the highest beam throughput is found when the center of the beam enters the deflector at the center of it's entrance. The voltage was found by testing different values and seeing how much the deflector was bending particles. An example of how the voltage affects the bending can be found in figure 13. The angle of the deflector varied between 0 and -2.1 degrees, which corresponds to the end of the deflector moving between 0 cm and 2.4 cm. In the real K130, the maximum that each end of the deflector can move is 2 cm in each direction. This means that some of the angles in the simulation are not possible in the real cyclotron. With the entrance of the

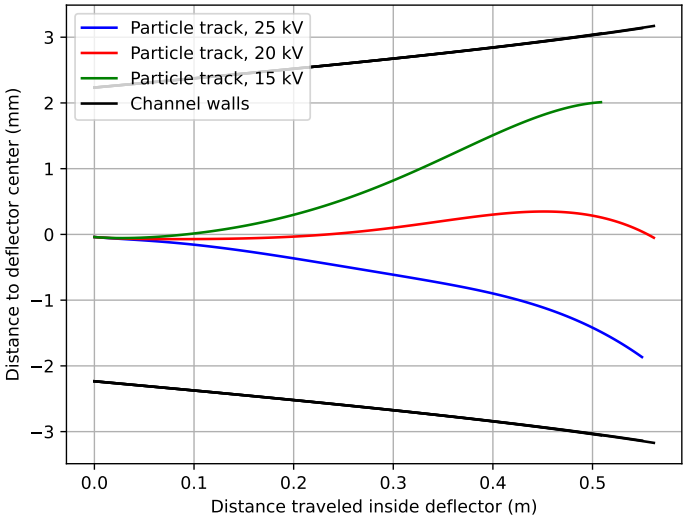

Figure 13. Here one can see the effect of the voltage on the bending of the particles inside the deflector. This example is made using $^{15}N^{4+}$ at roughly 130 MeV and a deflector angle of -1.2 degrees. The upper channel wall is the positive electrode and the lower channel wall is the negative electrode. The magnetic field bends the particles in roughly the opposite direction as the electric field.

deflector located at $r = 96.5$ cm, the limit on the angle is -1.7 degrees.

Once the optimal deflector angles were found for each case, multiple particles were calculated for each case. The particles were set to form a beam ellipse in (r, p_r) space around the optimal particle, i.e. the particle that hits the center of the deflector at both ends, with r corresponding to the radius and p_r being the radial velocity of the particles. With multiple particles one can rank the solutions based on the amount of particles passing through the deflector. Also the particles position and velocity are saved each orbit to plotting each particles journey in (r, p_r) space through the cyclotron and observe how the beam ellipse behaves during the last few turns. The starting beam ellipse can be seen in figure 14. The shape and size of the beam ellipse used for multiparticle analysis, was calculated from the assumption that at the entrance of the cyclotron the emittance, i.e. the area inside the ellipse, is 100 mm×mrad at 40 keV, then calculating the emittance at 55 MeV, i.e. roughly the starting energy in the simulation, gives an emittance of approximately 2.7 mm×mrad.

It can be seen from the results, that many otherwise good cases fail to be within the angle limit of the cyclotron. This leaves cases 6 and 14 that are over 130 MeV and inside the deflector limit. The (r, p_r) plots of these can be seen in figures 18 and

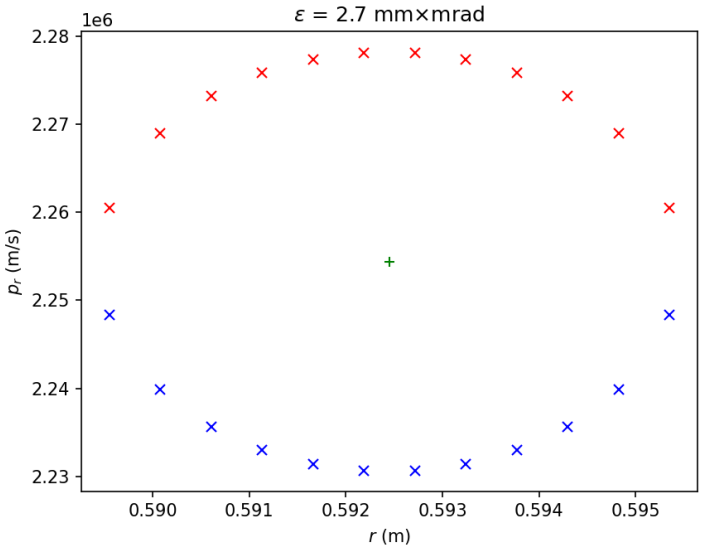

Figure 14. The starting beam ellipse used for analysis in phase space. Red and blue crosses represent particles on edge of the ellipse and the green plus sign denotes the center. The angle at which this ellipse is located is 270°.

19. In addition to the previous, two other plots, figures 17 and 20, were made to see how the particles behave at settings with lower energies.

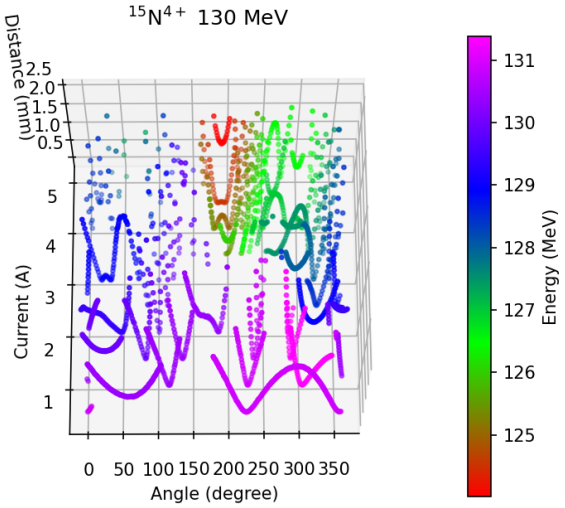

Figure 15. Full range of harmonic coil settings. Z-axis describes the distance to the center of the entrance to the deflector.

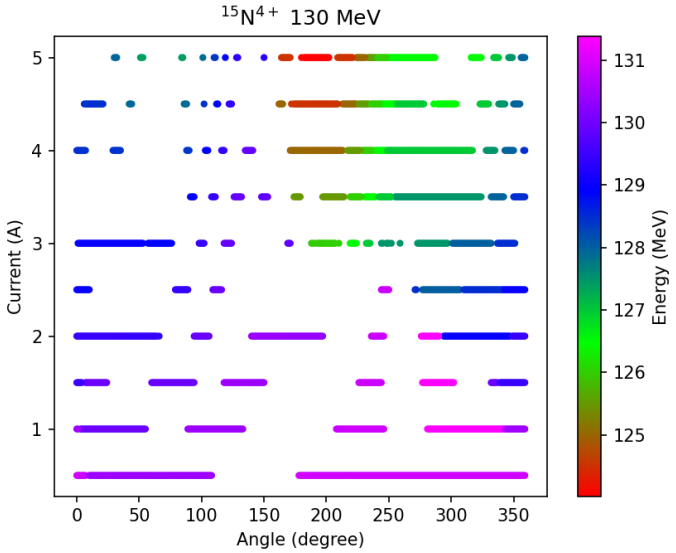

Figure 16. Figure showing the same data as figure 15, but with the z-axis removed.

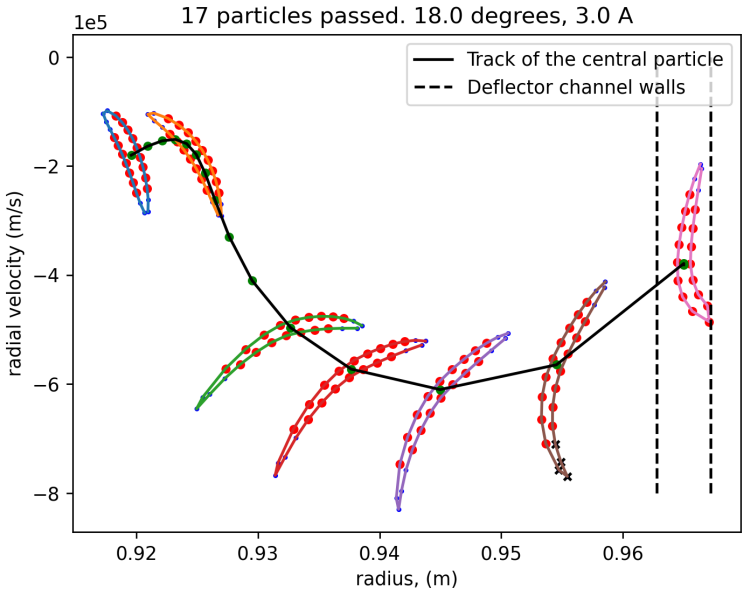

Figure 17. The (r, p_r) plot of the final 15 turns for case 0, from appendix A table 1, with $^{15}N^{4+}$. The amount of particles passed through the deflector as well as the harmonic coil settings are in the title of the figure. The blue dots represent particles that do not pass the deflector and the red dots represent particles that pass the deflector. The angle at which the phase space pattern is located is always at 8.8°, the same angle as the entrance to the deflector. The center of the entrance to the deflector is located at a radius of 96.5 cm. Here the radial turn separation seems to be quite large between the turns. The phase space pattern of the particles seems to elongate in velocity, but stays well intact in the radial direction.

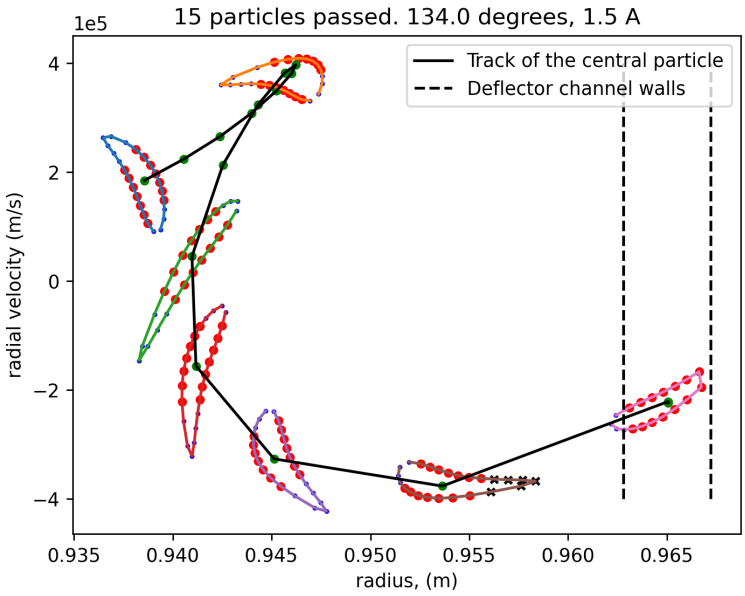

Figure 18. The (r, p_r) plot of the final 15 turns for case 6, from appendix A table 1, with $^{15}N^{4+}$. It seems that in this case the center of the phase space pattern performs a loop in phase space during the final few turns. Here the loop is quite small. The turn separation during the last turns is quite large.

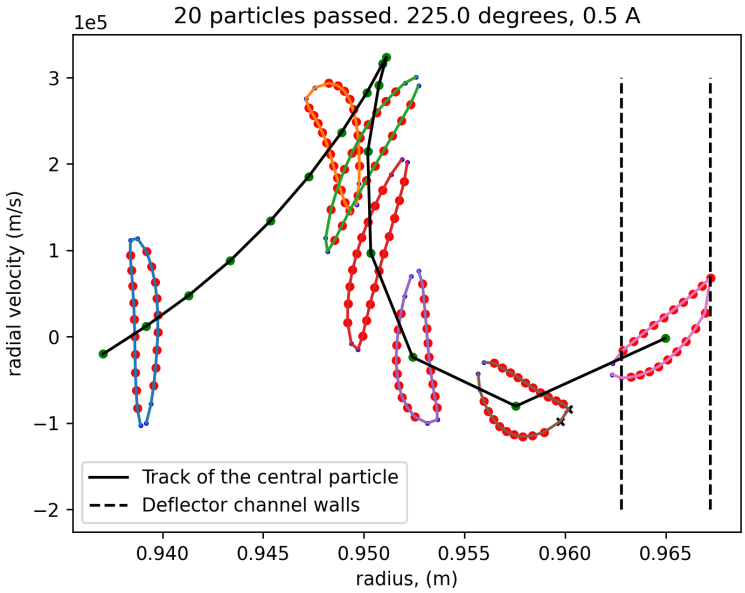

Figure 19. The (r, p_r) plot of the final 15 turns for case 14, from appendix A table 1, with $^{15}N^{4+}$. Here one can see a similar phase space loop as in figure 18. The beam ellipse shape is maintained quite well and the radial separation of the final few turns is not as great as in case 6.

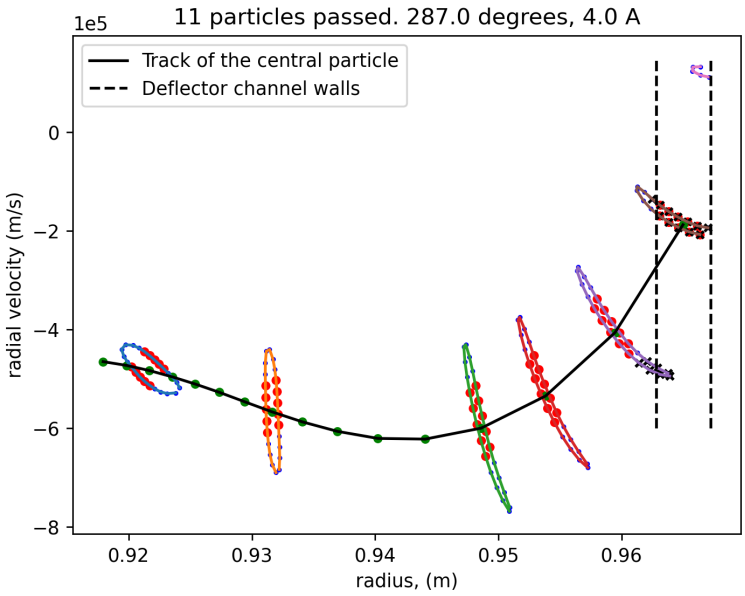

Figure 20. The (r, p_r) plot of the final 15 turns for case 20, from appendix A table 1, with $^{15}N^{4+}$. In this figure one can see that there is no loop or bump like in the other figures and the particles are extracted at the maximum radial velocity. Also the last few turns have very small turn separation, making the extraction inefficient.

4.2 Argon at 140 MeV

The accelerated particle analyzed in the second case was $^{36}Ar^{7+}$ with a target energy of 140 MeV. This was chosen because the data for it was easily available as it was recently used, so a direct comparison could be done to see if the settings in real life were comparable to the simulation and if so, are the settings used optimal. One problem with this case was that there was no way to get the trim coil currents from the real life run exactly the same as in the simulation. Otherwise the currents were roughly the same, but the last coil in real life had a current of 12.68 A and in the simulation 0 A. With the real life trim coil currents the phase error would get too high and no amount of tuning the acceleration frequency could fix the issue. Therefore trim coil currents and acceleration frequency from Fielder were used in the simulation. The reason for this discrepancy could be caused by many reasons, e.g. the interpolation of the magnetic field, imperfections in the real cyclotron, the values in the operating system not being entirely accurate, etc. Even though the settings are not exactly identical there should be enough similarities between the simulation and real life that a qualitative comparison can be done. Even though the magnetic field is not the same, the position and voltage of the deflector were set to be the same as in real life. The relevant settings from the real life run can be found in appendix B.

As with the $^{15}N^{4+}$ case, the first step was to iterate through the combinations of currents and angles of the harmonic coils. For this step a time step of 5×10^{10} was used to speed up the iteration. From this we get figures 21 and 22. Looking at the figure one can see that 140 MeV is not quite reached at any point. This probably stems from the magnetic field being weaker than in real life, and the deflectors entrance being closer to the center. In contrast to the $^{15}N^{4+}$ case, the deflector was turned away so that more particles would make it to the entrance of the deflector. This is why the figure is more densely populated.

Looking at the figure it was determined that the best cases were located between 100–160 degrees and 0.5–1.0 A. This region was then swept through with a smaller current step and so figure 23 was created. From this figure we see that there are multiple solutions of angle and current, so that a particle from an equilibrium orbit hits the center of the entrance to the deflector. These solutions also have roughly similar energies, which of course is to be expected as the amount of orbits is the same.

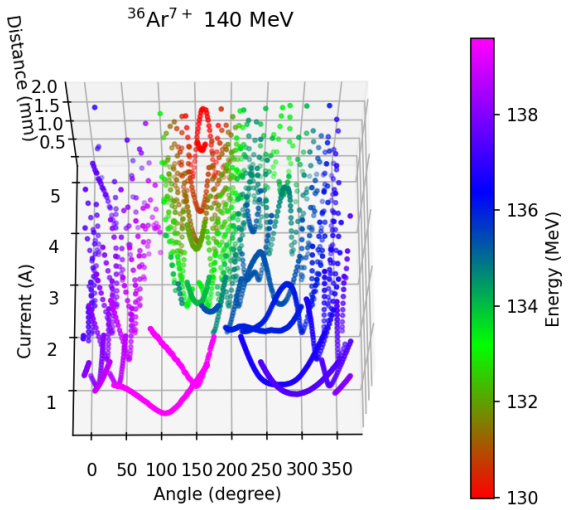

Figure 21. 4D plot showing energies and distance to the center of the deflector entrance as a function of harmonic coil angle and current.

From these solutions 32 were chosen as the best, i.e. the ones that enter the deflector closest to the center, to be analysed with multiple particles. This means that for all currents, multiple angles are considered to see if there is angular improvement in the passing of particles.

However before multiple particles were analyzed, the optimal angle of the deflector was calculated for each case. These angles varied between -1.60 to -1.27 degrees, both being inside the range of the real system. These angles of course depend on the voltage, so even if they were outside the range the voltage of the deflector could be set in a way that brings the angles back in range. In the real cyclotron the angle is -0.38 degrees. This difference can be due to the stronger magnetic field or maybe the position or voltage of the deflector is not quite accurate. It also might be that the position of the deflector is not exactly the same in the simulation as in real life. Nevertheless the results from the multiple particle simulation should be valid but need to be taken with a grain of salt due to the differing parameters in the simulation and real life.

The shape of the beam ellipse is as in figure 14, but the starting position in phase space and the emittance are different, the emittance being 3.6 mm×mrad. The calculation was the same as in the previous simulation except the energy at the cyclotron injection was assumed to be 70 keV. The particles on the edge, and one in

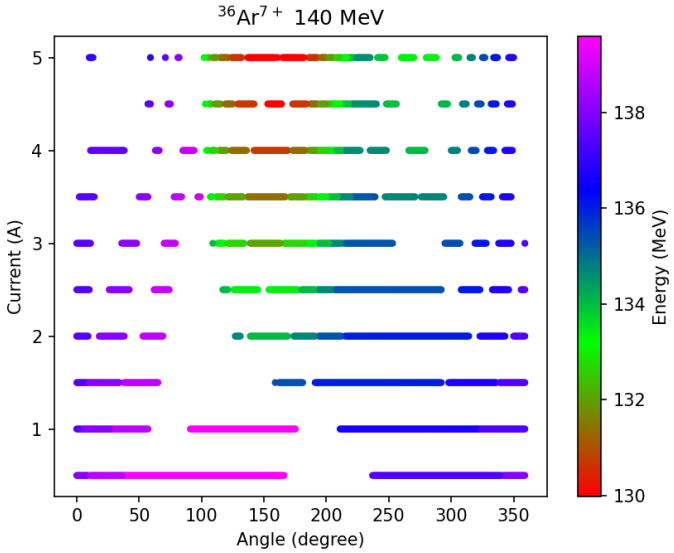

Figure 22. 3D plot showing the energies as a function of harmonic coil angle and current.

the center, of the beam ellipse were then simulated through the cyclotron and the amount of particles passing through deflector and their energies were saved. These results can be found in appendix A table 2. From the results it can be seen that more particles seem to pass the deflector with lower current and angle values. A few beam ellipse paths have been plotted in figures 24, 25 and 26 to show how the beam ellipses behave in the last few turns. The reason the central particle does not hit the center of the deflector in these figures is most likely due to a smaller time step used in the multiparticle simulation than in the harmonic coil settings iteration.

From the results the case in figure 24 was chosen for further analysis. This time the angle of the deflector was set at -1.6 degrees and multiple particles were simulated using harmonic coil current and angle combinations from around case 0 from appendix A table 2. From the results a contour plot was made, shown in figure 27. This was done to see how big the sensitivity to harmonic coil settings is in the amount of particles passing through. This is essentially how the K130 operator tunes the cyclotron. A few plots were made from the best cases and the worst cases seen in figures 28, 29 and 30. Note that in these figures the full acceptance is calculated using the energy of the central particle of the case in figure 24.

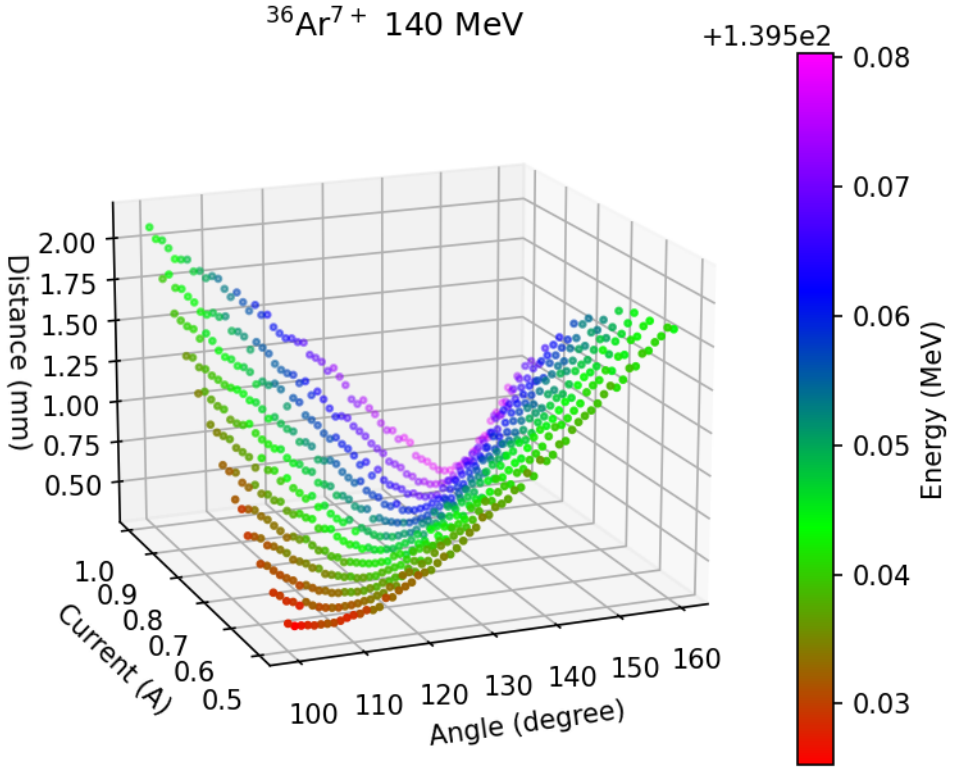

Figure 23. The range of angles and currents chosen for closer analysis.

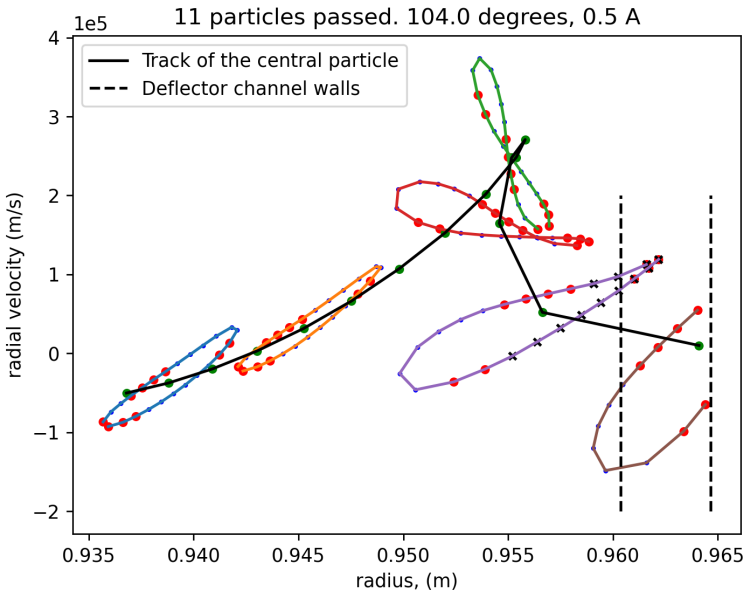

Figure 24. The (r, p_r) plot of the beam ellipse during the final few turns of case 0, from appendix A table 2, with $^{36}Ar^{7+}$. The radius and radial velocity are captured at 8.8°, the same angle as the entrance of the deflector. Red circles are the particles that pass through the deflector and blue circles hit the wall at some point. The green circle is the particle that starts exactly at the equilibrium orbit and the black line is the path of it. If a particle hits a wall or exits the deflector before the ideal particle, a black cross marks the final coordinates of it. This is the case with the most particles making it through the deflector.

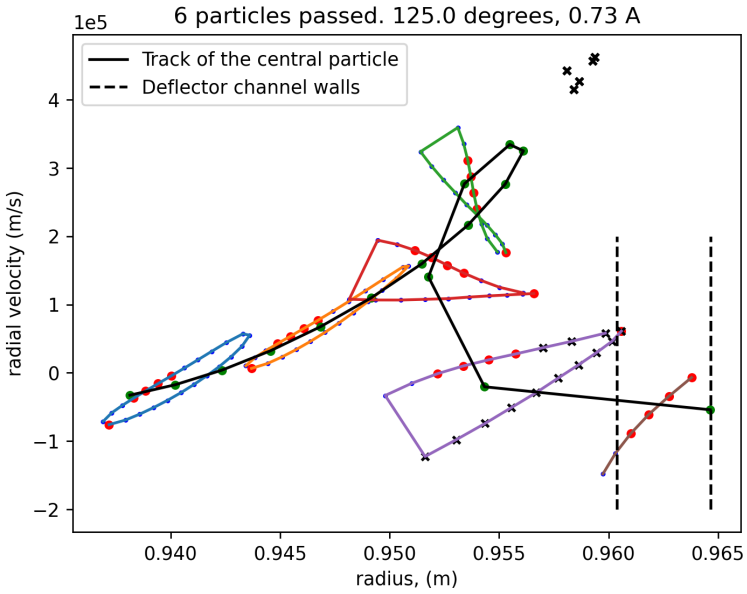

Figure 25. Case 17, from appendix A table 2. These setting produce a large loop in the (r, p_r) coordinates. Also some particles hit the wall very early.

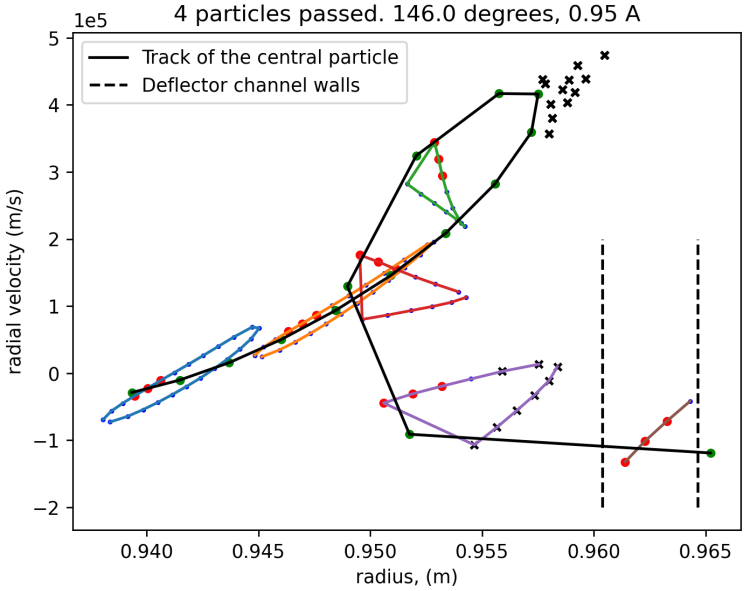

Figure 26. Case 29, from appendix A table 2. These settings produce an even larger loop than in figure 25. More particles hit the walls at an earlier time and very few particles make it through the deflector.

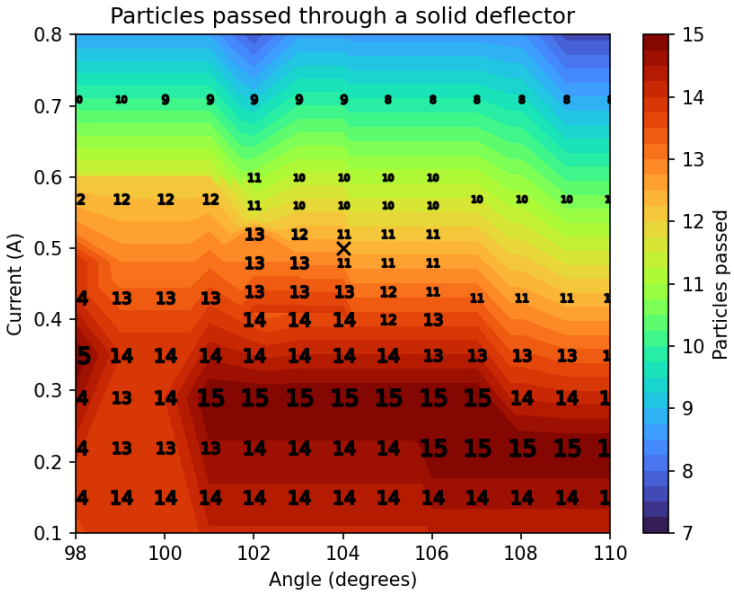

Figure 27. A contour plot showing the amount of particles as a function of both the harmonic coil angle and current. The data for this is found in appendix A table 3. The data is interpolated to the nearest point. The numbers mark the points used to make the contour plot and the cross marks the best settings from the harmonic coil sweep. Note that the integration time step here is smaller than in the full sweep to provide more accurate results.

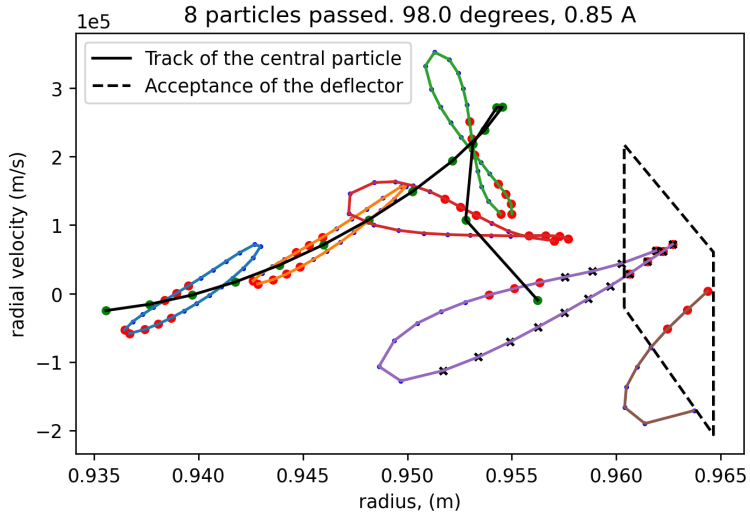

Figure 28. Case 0 from appendix A, table 3. Very few particles make it through as the emittance ellipse hits low in the acceptance range of the deflector. Note also that most particles that pass, do so in the second to last turn. The area of the acceptance of the deflector is roughly 40 mm×mrad.

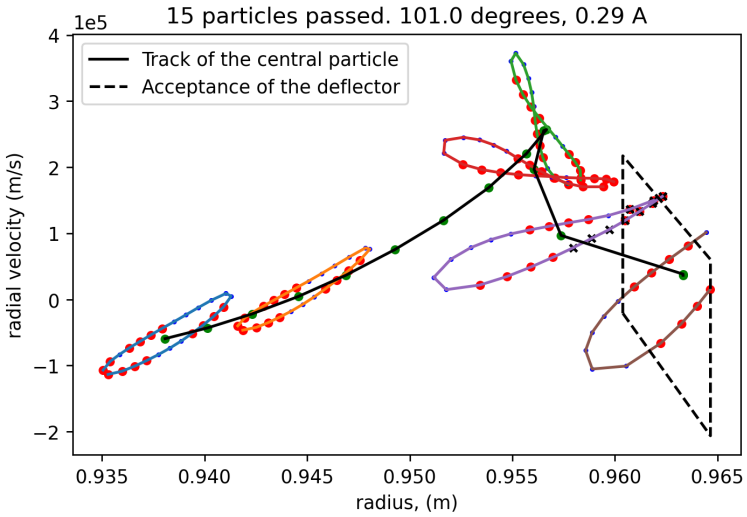

Figure 29. Case 31 from appendix, A table 3. One of the best cases. The particles have a much smaller beam ellipse on the last few turns, than in the bad cases. There are few particles that extract one turn too early. The center of the beam ellipse also fits nicely in the center of the acceptance. Note that the acceptance range is only meaningful during the last turn as there is a difference in energy each turn. However the energy increase is quite small so the second to last turn will have a roughly similar acceptance.

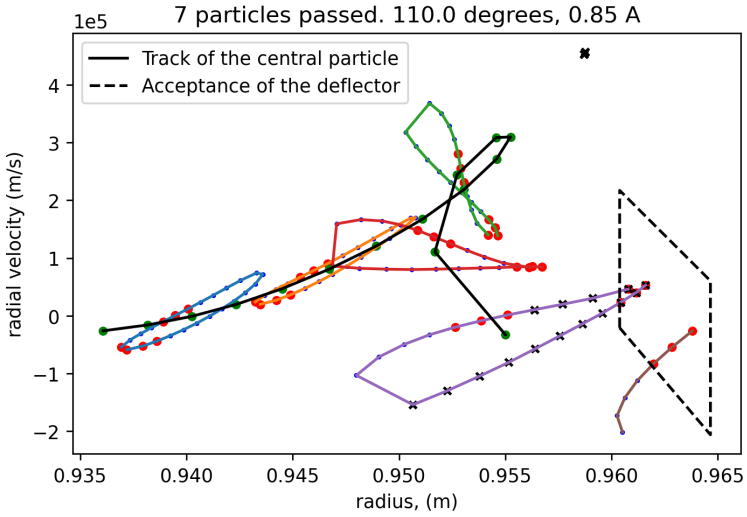

Figure 30. Case 145 from appendix A, table 3. The absolute worst case. As can be seen some particles are terminated very early. The beam ellipse is much larger than in the good cases, and seems to just be inside the acceptance during the final turn.

5 Conclusions

The purpose of this study was to find out if the operators can adjust the settings of the cyclotron so that the extraction is as optimal as it can be. From the two cases studied, it would seem that the harmonic coils have a small area of angle and current values, that extract the maximum amount of particles, as can be seen in figure 27. With the testing done, it can be seen that these settings are within the tuning limits of the real cyclotron. Of course the simulation is not entirely accurate to the real cyclotron, as can be seen by the difference of simulation parameters and real life parameters, but from the two cases studied, it would seem that there is only one valley of good harmonic coil settings for each field that produces the target energy. From the results it seems that for the magnetic fields that Fielder outputs, the target energy for the particles arises when harmonic coil currents are low and the angle is between 50 and 150 degrees in the simulation. This can be seen in the cases for both particles.

With different magnetic fields the optimal settings change, and as can be seen from the results, the harmonic coils can be used to adjust the energies, i.e. the number of turns the particles make around the cyclotron. It is possible that with a different combination of magnetic field and harmonic coil settings, there is a better output of particles. Something relating to this can be seen in figure 15. As can be seen from the figure, some settings give lower energies than desired, but have multiple particles passing through the deflector. And in figure 27 it can be seen that there indeed is a relatively large area where the number of particles passing the deflector is greater than in the surrounding area. Verifying this would require many more simulations with different magnetic fields, but might show that the real extraction from the cyclotron can be improved. Also testing should be done using particles in different acceleration phases. This would give more info about the particle output and might make some harmonic coil settings better.

The biggest problem in studying the extraction, is that there are so many adjustable settings that affect the effectiveness of the extraction. Doing a sweep of the harmonic coil settings in a 2-dimensional simulation already takes a lot of

time and adding, for example, a sweep of the deflector settings would be very time consuming indeed. As can be seen from figures 28, 29 and 30, the beam shape does not match the acceptance of the deflector. There might be some trim coil or injection settings with which one could compress the beam ellipse in such a way that it would fit nicely inside the acceptance. However in reality and in the simulation, finding the optimal beam shape is most likely impossible due to the aforementioned number of adjustable parameters.

It most likely would be better to write the simulation code in C++ or other compiled language as it most likely would speed up the simulations considerably. This would also allow the simulation to be run with a smaller time step, thereby increasing the accuracy. There are also improvements that could be made to improve the accuracy of the simulation, such as a more accurate simulation of the magnetic field, modeling the dee-electrodes to match their real life counterparts, making a more accurate representation of the deflector, including the central region of the cyclotron, introducing three dimensions into the simulation, etc. However for the purpose of this study the code was sufficient as is. The solid deflector analysis would also greatly benefit from having a faster runtime, since the accuracy of the range of good cases increases with the number of simulated particles and harmonic coil settings. Looking at figure 29, a better way to analyse the amount of particles might be to check how big of an area of the total ellipse is inside the acceptance of the deflector during the final turn. This requires the same amount of particles as these simulations but would give out a result that is more in line with real life. Also it would be best to keep the time step constant during all steps of the analysis, since it has a big effect on how accurate the simulation is. In the argon simulation, the larger time step used in the harmonic coil sweep means that the trajectory of the central particle is not as accurate. This causes an inaccuracy, as can be seen in figures 24, 25 and 26, which were made using a smaller time step, where the particles do not hit the center of the deflector channel as they should. The analysis with the solid deflector still stands true even if the selection of the harmonic coil settings was not entirely accurate.

At least for the cases simulated, it would seem that the way the operators set the values of the cyclotron is optimal in the case of the harmonic coil settings, as there is a clear region of target energy and high output of particles. And as can be seen from figure 27 the range of cases with the maximum particle output is large

enough that the operator can accurately find it.

The results for the simulations are in appendix A. The code and the data from the simulation is available at `https://gitlab.jyu.fi/tilaanah/gradukoodit`.

References

[1] E. O. Lawrence and M. S. Livingston. "The Production of High Speed Light Ions Without the Use of High Voltages". In: *Phys. Rev.* 40 (1 Apr. 1932), pp. 19–35. DOI: 10.1103/PhysRev.40.19. URL: https://link.aps.org/doi/10.1103/PhysRev.40.19.

[2] P. Heikkinen and E. Liukkonen. "Cyclotron development program at Jyväskylä". In: *AIP Conference Proceedings* 600.1 (Dec. 2001), pp. 89–93. ISSN: 0094-243X. DOI: 10.1063/1.1435204. eprint: https://pubs.aip.org/aip/acp/article-pdf/600/1/89/12144117/89_1_online.pdf. URL: https://doi.org/10.1063/1.1435204.

[3] P. Heikkinen and E. Liukkonen. "K130 Cyclotron - The First Years of Full Operation". In: *14th International Conference on Cyclotrons and Their Applications*. Aug. 1996, pp. 66–69.

[4] M. Livingston and J. Blewett. *Particle Accelerators*. International series in pure and applied physics. McGraw-Hill, 1962. URL: https://books.google.fi/books?id=Bz2BAAAAIAAJ.

[5] J. I. M. Botman and H. L. Hagedoorn. "Extraction from cyclotrons". In: (1996). DOI: 10.5170/CERN-1996-002.169. URL: http://cds.cern.ch/record/399427.

[6] L. H. Thomas. "The Paths of Ions in the Cyclotron I. Orbits in the Magnetic Field". In: *Phys. Rev.* 54 (8 Oct. 1938), pp. 580–588. DOI: 10.1103/PhysRev.54.580. URL: https://link.aps.org/doi/10.1103/PhysRev.54.580.

[7] S. Zaremba and W. Kleeven. "Cyclotrons: Magnetic Design and Beam Dynamics". en. In: *CERN Yellow Reports: School Proceedings* (2017), Vol 1 (2017): Proceedings of the CAS–CERN Accelerator School on Accelerators for Medical Applications. DOI: 10.23730/CYRSP-2017-001.177. URL: https://e-publishing.cern.ch/index.php/CYRSP/article/view/99.

[8] V. Bechtold. “Commercially Available Compact Cyclotrons for Isotope Production”. In: *13th International Conference on Cyclotrons and Their Applications*. Mar. 1993, p. II01.

[9] A. I. Papash and Y. G. Alenitsky. “Commercial cyclotrons. Part I: Commercial cyclotrons in the energy range 10–30 MeV for isotope production”. In: *Physics of Particles and Nuclei* 39.4 (July 2008), pp. 597–631. ISSN: 1531-8559. DOI: 10.1134/S1063779608040060. URL: https://doi.org/10.1134/S1063779608040060.

[10] W. Kleeven et al. “The self-extracting cyclotron”. In: *AIP Conference Proceedings* 600.1 (Dec. 2001), pp. 69–73. ISSN: 0094-243X. DOI: 10.1063/1.1435200. eprint: https://pubs.aip.org/aip/acp/article-pdf/600/1/69/12144388/69_1_online.pdf. URL: https://doi.org/10.1063/1.1435200.

[11] P. C. Y. Jongen D. Vandeplassche. “High Intensity Cyclotrons for Radioisotope Production, or The Comeback of the Positive Ions”. In: *Proc. 14th Int. Conf. on Cyclotrons and theirApplications*. Cape Town, South Africa: World Scientific Publishing Co. Pte. Ltd, Oct. 1995, pp. 115–119.

[12] E. Liukkonen. “New K130 Cyclotron at Jyväskylä”. In: *13th International Conference on Cyclotrons and Their Applications*. July 1992, pp. 22–27.

[13] P. Heikkinen. “The Jyväskylä K130 Cyclotron Magnet”. In: *12th International Conference on Cyclotrons and Their Applications*. May 1989, pp. 464–466.

[14] M. Gordon and D. F. Johnson. “Application of a new field trimming program to the MSU Cyclotron”. In: *AIP Conference Proceedings* (Jan. 1972). DOI: 10.1063/1.2946373. URL: https://doi.org/10.1063/1.2946373.

[15] Dassault Systèmes. *Opera Simulation Software*. Version 19. URL: https://www.3ds.com/products/simulia/opera.

[16] C. R. Harris et al. “Array programming with NumPy”. In: *Nature* 585.7825 (Sept. 2020), pp. 357–362. DOI: 10.1038/s41586-020-2649-2. URL: https://doi.org/10.1038/s41586-020-2649-2.

[17] P. Virtanen et al. “SciPy 1.0: Fundamental Algorithms for Scientific Computing in Python”. In: *Nature Methods* 17 (2020), pp. 261–272. DOI: 10.1038/s41592-019-0686-2.

[18] D. Meeker et al. “Finite element method magnetics”. In: *FEMM* 4.32 (2010), p. 162.

A Simulation result tables

Table 1. Results for $^{15}N^{4+}$ at target energy of 130 MeV

	harm angle (degrees)	harm current (A)	defl angle (degrees)	particle count	ave energy (MeV)	max energy (MeV)	min energy (MeV)
0	18.0	3.0	-0.839	17	128.967643	129.005807	128.927941
1	46.0	2.0	-1.032	15	129.460604	129.486081	129.433576
2	47.0	2.0	-1.020	14	129.460748	129.486148	129.434138
3	82.0	1.5	-1.223	11	129.940333	129.952605	129.922654
4	93.0	3.5	-0.195	2	128.914832	128.923210	128.906454
5	100.0	3.0	-0.580	5	129.425964	129.441399	129.409438
6	134.0	1.5	-1.200	15	130.408183	130.435344	130.383214
7	150.0	3.5	-0.417	10	125.450996	125.994720	124.999520
8	181.0	4.0	-2.035	6	124.585545	124.590487	124.580055
9	185.0	4.5	-2.094	6	124.323763	124.599084	124.047829
10	186.0	2.0	-0.818	12	126.417310	126.505953	125.996660
11	186.0	4.5	-2.088	7	124.362043	124.599624	124.048579
12	197.0	3.5	-2.087	6	125.065035	125.067209	125.062716
13	219.0	4.5	-2.086	17	124.958837	125.068915	124.505155
14	225.0	0.5	-1.561	20	130.900213	130.926988	130.874019
15	230.0	4.5	-2.102	16	125.474806	125.560261	124.994586
16	247.0	2.5	-1.126	0	0.000000	0.000000	0.000000
17	251.0	4.0	-2.098	22	127.029963	127.054885	127.009121
18	268.0	3.5	-1.878	21	127.503297	127.516548	127.490370
19	269.0	3.5	-1.852	21	127.502618	127.515855	127.489881
20	287.0	4.0	-0.941	11	127.011169	127.016824	127.004818
21	305.0	1.0	-1.748	19	131.304492	131.408518	130.912908
22	308.0	4.0	-0.582	7	127.010707	127.019087	127.003298
23	327.0	2.5	-1.514	18	128.507121	129.014328	127.932238
24	338.0	3.5	-0.936	10	127.882940	128.009556	127.442857
25	341.0	4.5	-0.464	8	127.363546	127.511544	126.950817
26	353.0	4.5	-0.588	9	127.867759	128.001022	127.451958
27	355.0	3.5	-0.948	12	128.392478	128.502927	127.951531
28	356.0	0.5	-1.879	23	130.849914	131.376713	130.387070
29	357.0	0.5	-1.885	22	130.846925	131.376206	130.386143

Table 2. Results for $^{36}Ar^{7+}$ at target energy of 140 MeV.

	harm angle (degrees)	harm current (A)	defl angle (degrees)	particle count	ave energy (MeV)	max energy (MeV)	min energy (MeV)
0	104.0	0.500000	-1.600	11	139.424161	139.648827	139.117376
1	105.0	0.500000	-1.595	11	139.424733	139.649181	139.117970
2	106.0	0.500000	-1.592	11	139.424776	139.649009	139.117340
3	107.0	0.500000	-1.585	11	139.426398	139.651441	139.119270
4	109.0	0.550000	-1.568	10	139.404207	139.651600	139.117614
5	110.0	0.550000	-1.562	10	139.405018	139.652116	139.118334
6	111.0	0.550000	-1.557	10	139.405852	139.654976	139.119475
7	112.0	0.550000	-1.549	10	139.407441	139.656734	139.121324
8	114.0	0.594444	-1.538	10	139.406774	139.655994	139.119148
9	115.0	0.594444	-1.529	10	139.408292	139.656787	139.119977
10	116.0	0.594444	-1.525	9	139.428089	139.658546	139.120121
11	117.0	0.638889	-1.508	9	139.429579	139.661243	139.120489
12	118.0	0.638889	-1.503	9	139.430133	139.660621	139.122181
13	119.0	0.638889	-1.500	9	139.430473	139.661730	139.121881
14	120.0	0.638889	-1.494	8	139.412408	139.663333	139.122411
15	122.0	0.683333	-1.474	7	139.455465	139.665790	139.229984
16	124.0	0.683333	-1.466	7	139.456395	139.666686	139.231264
17	125.0	0.727778	-1.446	6	139.492475	139.670849	139.230958
18	126.0	0.727778	-1.445	6	139.492819	139.670571	139.231551
19	127.0	0.727778	-1.438	6	139.494147	139.671805	139.232201
20	129.0	0.772222	-1.416	5	139.549287	139.676308	139.435510
21	130.0	0.772222	-1.413	5	139.549483	139.676480	139.436143
22	133.0	0.816667	-1.382	5	139.554213	139.682935	139.441032
23	134.0	0.816667	-1.382	5	139.554240	139.682483	139.440999
24	136.0	0.861111	-1.361	5	139.558172	139.687761	139.444809
25	137.0	0.861111	-1.355	5	139.559118	139.689122	139.444539
26	141.0	0.905556	-1.325	5	139.563887	139.694580	139.450111
27	142.0	0.905556	-1.322	5	139.564626	139.695474	139.451461
28	145.0	0.950000	-1.300	4	139.596615	139.701780	139.501293
29	146.0	0.950000	-1.291	4	139.598740	139.703067	139.503665
30	149.0	1.000000	-1.267	4	139.603749	139.710860	139.509146
31	150.0	1.000000	-1.267	3	139.634711	139.709604	139.565007

Table 3. Results for $^{36}Ar^{7+}$ at target energy of 140 MeV. This time with a solid deflector to see how big the area of maximum particles exiting the cyclotron is. The deflector angle is set at -1.6 degrees as in case 0 in 2.

	harm angle (degrees)	harm current (A)	defl angle (degrees)	particle count	ave energy (MeV)	max energy (MeV)	min energy (MeV)
0	98.0	0.85	-1.6	8.0	139.288887	139.517191	139.099174
1	98.0	0.15	-1.6	14.0	139.452766	139.842608	138.526206
2	98.0	0.22	-1.6	14.0	139.399530	139.786388	138.517835
3	98.0	0.29	-1.6	14.0	139.449720	139.783971	139.013362
4	98.0	0.35	-1.6	15.0	139.406366	139.719721	139.008409
5	98.0	0.43	-1.6	14.0	139.380261	139.655022	139.002834
6	98.0	0.57	-1.6	12.0	139.351663	139.652579	138.992509
7	98.0	0.71	-1.6	10.0	139.290601	139.561380	138.982932
8	98.0	0.05	-1.6	13.0	139.464328	139.844493	138.430285
9	99.0	0.85	-1.6	8.0	139.288503	139.515658	139.098302
10	99.0	0.15	-1.6	14.0	139.452667	139.843760	138.525367
11	99.0	0.22	-1.6	13.0	139.397301	139.784841	138.518908
12	99.0	0.29	-1.6	13.0	139.441115	139.785184	139.012800
13	99.0	0.35	-1.6	14.0	139.407694	139.718086	139.007900
14	99.0	0.43	-1.6	13.0	139.379952	139.655125	139.001491
15	99.0	0.57	-1.6	12.0	139.351051	139.653764	138.992106
16	99.0	0.05	-1.6	14.0	139.397901	139.845290	138.430104
17	99.0	0.71	-1.6	10.0	139.290302	139.562572	138.982930
18	100.0	0.05	-1.6	14.0	139.397888	139.844725	138.430281
19	100.0	0.22	-1.6	13.0	139.466998	139.785865	139.019581
20	100.0	0.29	-1.6	14.0	139.449225	139.783540	139.011959
21	100.0	0.35	-1.6	14.0	139.407780	139.718410	139.007720
22	100.0	0.43	-1.6	13.0	139.379541	139.655328	139.000992
23	100.0	0.57	-1.6	12.0	139.350149	139.651456	138.990319
24	100.0	0.71	-1.6	9.0	139.323801	139.561930	139.105750
25	100.0	0.85	-1.6	8.0	139.287523	139.515388	139.097323
26	100.0	0.15	-1.6	14.0	139.452401	139.844200	138.524924
27	101.0	0.05	-1.6	14.0	139.398099	139.845332	138.429880
28	101.0	0.71	-1.6	9.0	139.322996	139.563053	139.104481
29	101.0	0.85	-1.6	8.0	139.286509	139.514995	139.096388
30	101.0	0.22	-1.6	13.0	139.466499	139.783472	139.018068
31	101.0	0.29	-1.6	15.0	139.435259	139.784100	139.012267
32	101.0	0.35	-1.6	14.0	139.407004	139.719206	139.007147
33	101.0	0.43	-1.6	13.0	139.378973	139.654757	139.002003
34	101.0	0.57	-1.6	12.0	139.349865	139.652104	138.990896
35	101.0	0.15	-1.6	14.0	139.452354	139.843751	138.525305
36	102.0	0.15	-1.6	14.0	139.452184	139.843187	138.526014
37	102.0	0.05	-1.6	14.0	139.397979	139.846128	138.430450
38	102.0	0.35	-1.6	14.0	139.406852	139.718061	139.007426
39	102.0	0.60	-1.6	11.0	139.380492	139.650502	139.111718
40	102.0	0.56	-1.6	11.0	139.382347	139.652177	139.113533
41	102.0	0.52	-1.6	13.0	139.374371	139.651964	138.993682
42	102.0	0.48	-1.6	13.0	139.376365	139.652913	138.997643
43	102.0	0.44	-1.6	13.0	139.378054	139.654948	138.999900
44	102.0	0.40	-1.6	14.0	139.404485	139.718856	139.003931
45	102.0	0.85	-1.6	7.0	139.301111	139.514065	139.095545
46	102.0	0.22	-1.6	14.0	139.452319	139.785151	139.018484
47	102.0	0.71	-1.6	9.0	139.322614	139.562636	139.102762
48	102.0	0.29	-1.6	15.0	139.435203	139.785229	139.012436
49	102.0	0.57	-1.6	11.0	139.381665	139.652447	139.113017
50	102.0	0.43	-1.6	13.0	139.378706	139.654408	139.000630
51	103.0	0.22	-1.6	14.0	139.452026	139.785368	139.018567
52	103.0	0.35	-1.6	14.0	139.406591	139.718088	139.007743
53	103.0	0.43	-1.6	13.0	139.378043	139.653433	139.000038
54	103.0	0.29	-1.6	15.0	139.434555	139.783049	139.011811
55	103.0	0.60	-1.6	10.0	139.398132	139.650404	139.110162
56	103.0	0.56	-1.6	10.0	139.399885	139.651947	139.112763
57	103.0	0.52	-1.6	12.0	139.405531	139.651853	139.115657
58	103.0	0.48	-1.6	13.0	139.375682	139.652054	138.997334
59	103.0	0.44	-1.6	13.0	139.377642	139.653685	138.999340
60	103.0	0.40	-1.6	14.0	139.403923	139.717426	139.003479
61	103.0	0.85	-1.6	8.0	139.317604	139.513123	139.094543
62	103.0	0.71	-1.6	9.0	139.365842	139.584547	139.103332
63	103.0	0.57	-1.6	10.0	139.400066	139.651200	139.113552
64	103.0	0.15	-1.6	14.0	139.452191	139.844120	138.525482
65	103.0	0.05	-1.6	14.0	139.398077	139.845151	138.431047
66	104.0	0.48	-1.6	11.0	139.425408	139.652637	139.118223
67	104.0	0.56	-1.6	10.0	139.399431	139.650187	139.112939
68	104.0	0.52	-1.6	11.0	139.423437	139.651126	139.115943
69	104.0	0.44	-1.6	13.0	139.377367	139.653395	138.999669
70	104.0	0.40	-1.6	14.0	139.403416	139.717032	139.001977
71	104.0	0.85	-1.6	8.0	139.317145	139.512478	139.093242
72	104.0	0.71	-1.6	9.0	139.365079	139.584425	139.102406
73	104.0	0.57	-1.6	10.0	139.399404	139.651361	139.111749

Table 4. Continuation of table 3

	harm angle (degrees)	harm current (A)	defl angle (degrees)	particle count	ave energy (MeV)	max energy (MeV)	min energy (MeV)
74	104.0	0.43	-1.6	13.0	139.377862	139.654063	138.999800
75	104.0	0.35	-1.6	14.0	139.406016	139.717279	139.006930
76	104.0	0.29	-1.6	15.0	139.434563	139.783689	139.011615
77	104.0	0.22	-1.6	14.0	139.451666	139.782967	139.017705
78	104.0	0.05	-1.6	14.0	139.397755	139.845441	138.429349
79	104.0	0.60	-1.6	10.0	139.397887	139.650738	139.108655
80	104.0	0.15	-1.6	14.0	139.451951	139.842379	138.526699
81	105.0	0.44	-1.6	12.0	139.390881	139.652107	138.998222
82	105.0	0.71	-1.6	8.0	139.339584	139.582638	139.102357
83	105.0	0.05	-1.6	14.0	139.398019	139.845371	138.430374
84	105.0	0.15	-1.6	14.0	139.451692	139.842920	138.526345
85	105.0	0.22	-1.6	14.0	139.451759	139.783363	139.016944
86	105.0	0.29	-1.6	15.0	139.434020	139.783147	139.011055
87	105.0	0.35	-1.6	14.0	139.405995	139.717651	139.006393
88	105.0	0.43	-1.6	13.0	139.416886	139.716178	139.000982
89	105.0	0.57	-1.6	10.0	139.398591	139.648946	139.111041
90	105.0	0.85	-1.6	8.0	139.316424	139.511041	139.091166
91	105.0	0.40	-1.6	12.0	139.406322	139.716834	139.003887
92	105.0	0.48	-1.6	11.0	139.425124	139.652230	139.118917
93	105.0	0.52	-1.6	11.0	139.423114	139.650758	139.114419
94	105.0	0.56	-1.6	10.0	139.399286	139.651279	139.111781
95	105.0	0.60	-1.6	10.0	139.397482	139.649419	139.109759
96	106.0	0.05	-1.6	14.0	139.397775	139.845461	138.429710
97	106.0	0.22	-1.6	15.0	139.477485	139.841452	139.017511
98	106.0	0.15	-1.6	14.0	139.451775	139.841601	138.524365
99	106.0	0.29	-1.6	15.0	139.433917	139.782961	139.011593
100	106.0	0.35	-1.6	13.0	139.420604	139.718310	139.005887
101	106.0	0.60	-1.6	10.0	139.396869	139.649980	139.107949
102	106.0	0.56	-1.6	10.0	139.398155	139.648592	139.111105
103	106.0	0.52	-1.6	11.0	139.422845	139.651573	139.114931
104	106.0	0.48	-1.6	11.0	139.424509	139.650639	139.118123
105	106.0	0.43	-1.6	11.0	139.426976	139.651612	139.122550
106	106.0	0.57	-1.6	10.0	139.398267	139.649938	139.111184
107	106.0	0.71	-1.6	8.0	139.339223	139.582927	139.100709
108	106.0	0.44	-1.6	11.0	139.426324	139.654136	139.120153
109	106.0	0.85	-1.6	8.0	139.315916	139.511048	139.092440
110	106.0	0.40	-1.6	13.0	139.417687	139.717487	139.002284
111	107.0	0.85	-1.6	8.0	139.315355	139.509938	139.090975
112	107.0	0.29	-1.6	15.0	139.433508	139.782271	139.009930
113	107.0	0.22	-1.6	15.0	139.477211	139.841395	139.017226
114	107.0	0.15	-1.6	14.0	139.451342	139.842004	138.525924
115	107.0	0.71	-1.6	8.0	139.338991	139.582617	139.100779
116	107.0	0.05	-1.6	14.0	139.397812	139.844823	138.429853
117	107.0	0.57	-1.6	10.0	139.397303	139.649112	139.109906
118	107.0	0.35	-1.6	13.0	139.419572	139.716891	139.005157
119	107.0	0.43	-1.6	11.0	139.426452	139.651355	139.121491
120	108.0	0.85	-1.6	8.0	139.315352	139.510230	139.089716
121	108.0	0.71	-1.6	8.0	139.338069	139.582651	139.100010
122	108.0	0.57	-1.6	10.0	139.397309	139.649372	139.109751
123	108.0	0.43	-1.6	11.0	139.426321	139.652221	139.122104
124	108.0	0.35	-1.6	13.0	139.419548	139.717578	139.005272
125	108.0	0.29	-1.6	14.0	139.448820	139.782462	139.011049
126	108.0	0.22	-1.6	15.0	139.477079	139.841781	139.015667
127	108.0	0.15	-1.6	14.0	139.451596	139.841578	138.525589
128	108.0	0.05	-1.6	14.0	139.397699	139.844422	138.430210
129	109.0	0.29	-1.6	14.0	139.448686	139.781613	139.010694
130	109.0	0.71	-1.6	8.0	139.337414	139.581810	139.099536
131	109.0	0.05	-1.6	14.0	139.397456	139.844631	138.429573
132	109.0	0.15	-1.6	14.0	139.451505	139.842432	138.525714
133	109.0	0.22	-1.6	15.0	139.476802	139.840586	139.017885
134	109.0	0.35	-1.6	13.0	139.419369	139.716786	139.004601
135	109.0	0.43	-1.6	11.0	139.425780	139.651087	139.120962
136	109.0	0.57	-1.6	10.0	139.396559	139.647285	139.109750
137	109.0	0.85	-1.6	7.0	139.295727	139.509574	139.089871
138	110.0	0.71	-1.6	8.0	139.336297	139.580538	139.097378
139	110.0	0.05	-1.6	14.0	139.397380	139.844871	138.431012
140	110.0	0.15	-1.6	14.0	139.451028	139.842508	138.525966
141	110.0	0.22	-1.6	15.0	139.476735	139.840131	139.017274
142	110.0	0.35	-1.6	12.0	139.453619	139.716981	139.127023
143	110.0	0.43	-1.6	11.0	139.425353	139.650644	139.120757
144	110.0	0.57	-1.6	10.0	139.396618	139.648802	139.109405
145	110.0	0.85	-1.6	7.0	139.294547	139.507747	139.088697
146	110.0	0.29	-1.6	14.0	139.448348	139.781793	139.010676

B Real life operational values for $^{36}Ar^{7+}$ at 140 MeV

JYFL

K130 Cyclotron
Operational Parameters

LogSheet Nr: A-47c/2023

18.12.2023

Ion	*Energy*	*User*	*Proposal ID*
36 Ar 7+	**140 MeV**	**Juromara**	JM38

Operator: Hyvonen Jani

Recipe: A-47c_2023_Argon_36_140MeV_MARA

ECR 2

Gas Controls	**Ion1 :** 36 Ar Pos: 1552	**Buffer:** N **Pos: 898**	**ECR Vacuum**	Injection vacuum: 1.9E-07 mbar		
				Extraction vacuum: 1.7E-07 mbar		
Pressure	Ion: 554 mbar	Bfr: 630 mbar		Bias	60 V	904 uA
RF Power	uWave: 101 W	**TWTA: 0 W**		Accel HV	8.13 kV	1.06 mA
Coils	COIL1: 489.7 A	COIL2: 500.0 A	**HV**	Puller HV	1.50 kV	0.29 mA
Dipole &	DJ1: 68.18 A	SOLJ1: 72.50 A		Einzel 1	7.00 kV	0.01 mA
Solenoids	SOLJ2: 39.60 A	SOLJ3: 47.30 A		~~Einzel 2~~	~~0.00 kV~~	~~0.01 mA~~
Steering	STJ1 X: 0.00 A	STJ1 Y: 0.00 A	**Electrodes**	~~E1: 105.00~~	~~E2: 105.00~~	
Magnets	STJ2 X: 0.00 A	STJ2 Y: 0.00 A	SWI1: 10.21 A			
Vacuum		BJ2: 6.3E-08 mbar	**Radiation**	GMF04: 0.12 uSv/h		

INJECTION LINE

	SOLI3: 37.40 A	QI1: 0.00 A	STI3 X: -0.80 A	STI3 Y: -1.64 A
	SOLI4: 41.94 A	QI2: 0.00 A	STI4 X: -1.04 A	STI4 Y: 0.65 A
Magnets	SOLI5: 39.99 A	QI3: 0.00 A		
	SOLI6: 45.15 A	QI4: 0.00 A	DI2: 45.37 A	
	SOLI7: 115.96 A			
Buncher	Main level: 6.3 %	Main phase: 4.3 %	Level diff.: 40.0 %	Phase diff.: 48.1 %
Inflector	Voltage (+): 1.437 kV		Voltage (-): -1.437 kV	I (leak): 0.002 mA
Vacuum	TI6: 2.4E-08 mbar	BI4: 2.1E-08 mbar	BI5: 2.2E-08 mbar	

CYCLOTRON

MAIN COIL: 727 A

HARMONIC COILS

Coil	Amplitude	Angle
A	1.65 A	250 deg
B		
C		
D	0.64 A	243 deg

Vacuum
Tank injection: 2.7E-08 mbar
Tank extraction: 8.0E-08 mbar
Liner: 9.1E-03 mbar

CRYC1: 13 K CRYC2: 14 K

TRIM COILS

1U	-15.80 A	8	+30.70 A
1L	-35.80 A	9	+42.30 A
2	-9.40 A	10	+29.60 A
3	-6.30 A	11	+56.10 A
4	-0.70 A	12	+87.90 A
5	+7.10 A	13	+44.90 A
6	+14.90 A	14	-4.10 A
7	+15.70 A	**15**	**+12.68 A**

Internal steering magnet (IX): 0.00 A

RF

Frequency	13.911 MHz		U-dee	Grid	Coarse	Fine	Coupling
Harmonic mode	3	**RF 1**	**29.4 kV**	730	1259 mm	232	397
Br		**RF 2**	**31.5 kV**	719	1249 mm	344	409

	I-ca	I-an	U-g1	I-g2	P-fwd.	P-refl.	Ur-an	Udee (R)	P-an
RF 1	197 A	2.2 A	0.315 kV	61 mA	151 W	4.4 W	4.2 kV	29.8 kV	9.26
RF 2	220 A	2.0 A	0.319 kV	50 mA	240 W	0.3 W	3.6 kV	30.8 kV	7.12

EXTRACTION

Deflector

Deflector Enter: -2.5 Deflector Exit: 1.9 Defl. U: 13.3 kV

Current: 0.043 mA Cooling water G: 0.1 uS Cooling water temp.: 22.6 C

EMC

EMC Exit: -4.1 EMC current: 0 A

EMC voltage: 10.9 V

EXTRACTION H- (FOIL 2)

End slide: 98.8 cm Cross slide: -1.9 cm